This DR item accompanies Nakanishi, A., Takahashi, N., Yamamoto, Y., Takahashi, T., Citak, S.O., Nakamura, T., Obana, K., Kodaira, S., and Kaneda, Y., 2018, Three-dimensional plate geometry and P-wave velocity models of the subduction zone in SW Japan: Implications for seismogenesis, *in* Byrne, T., Underwood, M.B., Fisher, D., McNeill, L., Saffer, D., Ujiie, K., and Yamaguchi, A., eds., Geology and Tectonics of Subduction Zones: A Tribute to Gaku Kimura: Geological Society of America Special Paper 534, p. 69–86, https://doi.org/10.1130/2018.2534(04).

Figure S1. First-arrival tomography results for profile SK03 off Cape Ashizuri, Shikoku: (a) First-arrival tomography; (b) checkerboard test results; and (c) traveltime residuals and traveltime fitting diagram for the entire profile. The horizontal axis indicates distance from the northwestern end of the profile. The vertical axis of (c) show the OBS numbers from north to south along the profile.

Figure S2. Pseudolayer structural analysis results for profile SK03 off Shikoku. Ray diagrams for the calculated arrivals and comparison of traveltime curves of observed and calculated traveltimes from the pseudolayer model for profile SK03 (shown in Figure 2) and reflection arrivals for (a) the plate interface and (b) the oceanic Moho interface. Observed and calculated traveltimes are shown in gray and black, respectively. Yellow circles show the locations of OBSs. The horizontal axis indicates distance from the northwestern end of the profile.

Figure S3-1. First-arrival tomography results for profile HY01 in the Hyuga-nada region off Kyushu: (a) First-arrival tomography; (b) checkerboard test results; and (c) traveltime fitting diagram for the entire profile. Pale colors in (a) indicate areas through which no seismic rays passed. The horizontal axis indicates distance from the southern end of the profile. The vertical axis of (c) show the OBS numbers from south to north along the profile.

Figure S3-2. Pseudolayer structural analysis results for profile HY01: (a) Pseudolayer model for the profile shown in Figure S3-1, including along the landward extension of the profile in the onshore area. The horizontal axis indicates distance from the southern end of the profile. The velocity structure beneath the onshore area was analyzed by using airgun shot data observed by two Hi-net stations along the profile extension. The seismic reflectivity image obtained by the traveltime mapping method is superimposed in grayscale. (b) Traveltime fitting diagram for the pseudolayer model considering crustal interfaces based on reflection phases observed as clear later arrivals along the onshore–offshore profile. The vertical axis of (b) show the OBS numbers from south to north along the profile.

Figure S4-1. First-arrival tomography results for profile HY02 in the Hyuga-nada region off Kyushu: (a) First-arrival tomography; (b) checkerboard test results; and (c) traveltime fitting diagram for the entire profile. Pale colors in (a) indicate areas through which no seismic rays passed. The horizontal axis indicates distance from the southern end of the profile. The vertical axis of (c) show the OBS numbers from south to north along the profile.

Figure S4-2. Pseudolayer structural analysis results for profile HY02: (a) Pseudolayer model for the profile shown in Figure S4-1, including along the landward extension in the onshore area. The horizontal axis indicates distance from the southern end of the profile. The velocity structure beneath the onshore area was analyzed by using airgun shot data observed by two Hi-net stations along the profile extension. The two thick lines show interfaces interpreted as the plate interface and the oceanic Moho. The seismic reflectivity image obtained by the traveltime mapping

method is superimposed in grayscale. (b) Traveltime fitting diagram for the pseudolayer model considering crustal interfaces based on reflection phases observed as clear later arrivals along the onshore–offshore profile. The vertical axis of (b) show the OBS and land station numbers from south to north along the profile.

Figure S5-1. First-arrival tomography results for profile HY03 in the Hyuga-nada region: (a) First-arrival tomography; (b) checkerboard test results; and (c) traveltime fitting diagram for the entire profile. The horizontal axis indicates distance from the southwestern end of the profile. Pale colors in (a) indicate areas through which no seismic rays passed. The vertical axis of (c) show the OBS numbers and southwest to northeast along the profile except for two OBSs located at the crosspoints with HY01 and HY02.

Figure S5-2. Pseudolayer structural analysis results for profile HY03: (a) Pseudolayer model for profile HY03 shown in Figure S5-1. The horizontal axis indicates distance from the southwestern end of the profile. The seismic reflectivity image obtained by the traveltime mapping method is superimposed in grayscale. (b) Traveltime fitting diagram for the pseudolayer model considering crustal interfaces based on reflection phases observed as clear later arrivals along the profile. The vertical axis of (b) show the OBS numbers from southwest to northeast along the profile except for two OBSs located at the crosspoints with HY01 and HY02.

Figure S6-1. First-arrival tomography results for profile HY04 in the Hyuga-nada region: (a) First-arrival tomography; (b) checkerboard test results; and (c) traveltime fitting diagram for the entire profile. The horizontal axis indicates distance from the southwestern end of the profile. Pale colors in (a) indicate areas through which no seismic rays passed. The vertical axis of (c) show the OBS numbers from southwest to northeast along the profile except for two OBSs located at the crosspoints with HY01 and HY02.

Figure S6-2. Pseudolayer structural analysis results for profile HY04: (a) Pseudolayer model for profile HY04 shown in Figure S6-1. The horizontal axis indicates distance from the southwestern end of the profile. The seismic reflectivity image obtained by the traveltime mapping method is superimposed in grayscale. (b) Traveltime fitting diagram for the pseudolayer model considering crustal interfaces based on reflection phases observed as clear later arrivals along the profile. The vertical axis of (b) show the OBS numbers from southwest to northeast along the profile except for two OBSs located at the crosspoints with HY01 and HY02.

Figure S7-1. First-arrival tomography results for profile SK04 off Shikoku: (a) First-arrival tomography; (b) checkerboard test results; and (c) traveltime fitting diagram for the entire profile. The horizontal axis indicates distance from the southern end of the profile. Pale colors in (a) indicate areas through which no seismic rays passed. The vertical axis of (c) show the OBS numbers from north to south along the profile.

Figure S7-2. Pseudolayer structural analysis results for profile SK04: (a) Pseudolayer model for the profile shown in Figure S7-1, including along the landward extension in the onshore area. The horizontal axis indicates distance from the southern end of the profile. The velocity structure beneath the onshore area was analyzed by using airgun shot data observed by six Hi-net stations along the profile extension. Observed data acquired by long-term OBSs deployed for seismic

observations along profile SK04 were also used to construct the layered model. The seismic reflectivity image obtained by the traveltime mapping method is superimposed in grayscale. (b) Traveltime fitting diagram for the pseudolayer model considering crustal interfaces based on reflection phases observed as clear later arrivals along the onshore–offshore profile. The vertical axis of (b) show the OBS and land station numbers from north to south along the profile except for two OBSs for long-term observation.

Figure S8-1. First-arrival tomography results for profile SK01 off Shikoku: (a) First-arrival tomography; (b) checkerboard test results: and (c) traveltime fitting diagram for the entire profile. The horizontal axis indicates distance from the northern end of the profile. Pale colors in (a) indicate areas through which no seismic rays passed. The vertical axis of (c) show the OBS numbers from north to south along the profile.

Figure S8-2. Pseudolayer structural analysis results for profile SK01: (a) Pseudolayer model for the profile shown in Figure S8-1, including along the landward extension in the onshore area. The horizontal axis indicates distance from the northern end of the offshore profile. The velocity structure beneath the onshore area was analyzed by using airgun shot data observed by five Hi-net stations along the profile extension. Observed data acquired by long-term OBSs deployed for seismic observation along profile SK01 were also used to construct the layered model. The seismic reflectivity image obtained by the traveltime mapping method is superimposed in grayscale. (b) Traveltime fitting diagram for the pseudolayer model considering crustal interfaces based on reflection phases observed as clear later arrivals along the onshore–offshore profile. The vertical axis of (b) show the OBS and land station numbers from north to south along the profile except for three OBSs for long-term observation.

Figure S9-1. First-arrival tomography results for profile SK05 off Shikoku: (a) First-arrival tomography; (b) checkerboard test results; and (c) traveltime fitting diagram for the entire profile. The horizontal axis indicates distance from the western end of the offshore profile. Pale colors in (a) indicate areas through which no seismic rays passed. Observed data acquired by long-term OBSs deployed for seismic observation along the profile were also used to construct the layered model. The vertical axis of (c) shows the OBS numbers from west to east along the profile except for seven OBSs for long-term observation.

Figure S9-2. Pseudolayer structural analysis results for profile SK05 off Shikoku: (a) Pseudolayer model for the profile shown in Figure S9-1. The horizontal axis indicates distance from the western end of the offshore profile. The seismic reflectivity image obtained by the traveltime mapping method is superimposed in grayscale. (b) Traveltime fitting diagram for the pseudolayer model considering crustal interfaces based on reflection phases observed as clear later arrivals along the profile. The vertical axis of (b) show the OBS numbers from west to east along the profile except for seven OBSs for long-term observation.

Figure S10-1. First-arrival tomography results for profile SK06 off Shikoku: (a) First-arrival tomography; (b) checkerboard test results; and (c) traveltime fitting diagram for the entire profile. The horizontal axis indicates distance from the western end of the offshore profile. Pale colors in (a) indicate areas through which no seismic rays passed. Observed data acquired by long-term OBSs deployed for seismic observation along the profile were also used to construct

the layered model. The vertical axis of (c) show the OBS numbers from west to east along the profile except for seven OBSs for long-term observation.

Figure S10-2. Pseudolayer structural analysis results for profile SK06: (a) Pseudolayer model for the profile shown in Figure S10-1. The horizontal axis indicates distance from the western end of the offshore profile. The seismic reflectivity image obtained by the traveltime mapping method is superimposed in grayscale. (b) Traveltime fitting diagram for the pseudolayer model considering crustal interfaces based on reflection phases observed as clear later arrivals along the profile. The vertical axis of (b) show the OBS numbers from west to east along the profile except for seven OBSs for long-term observation.

Figure S11-1. First-arrival tomography results for profile SK07 off Shikoku: (a) First-arrival tomography; (b) checkerboard test results; and (c) traveltime fitting diagram for the entire profile. The horizontal axis indicates distance from the western end of the offshore profile. Pale colors in (a) indicate areas through which no seismic rays passed. Observed data acquired by long-term OBSs deployed for seismic observation along the profile were also used to construct the layered model. The vertical axis of (c) show the OBS numbers from west to east along the profile except for five OBSs for long-term observation.

Figure S11-2. Pseudolayer structural analysis results for profile SK07: (a) Pseudolayer model for the profile shown in Figure S11-1. The horizontal axis indicates distance from the western end of the offshore profile. The seismic reflectivity image obtained by the traveltime mapping method is superimposed in grayscale. (b) Traveltime fitting diagram for the pseudolayer model considering crustal interfaces based on reflection phases observed as clear later arrivals along the profile. The vertical axis of (b) show the OBS numbers from west to east along the profile except for five OBSs for long-term observation.

Figure S12. First-arrival tomography results for profile TK02 off the Kii Channel: (a) First-arrival tomography results. Yellow circles indicate OBSs. The horizontal axis indicates distance from the southern end of the offshore profile. The seismic reflectivity image obtained by the traveltime mapping method is superimposed in grayscale. The blue line shows the plate boundary according to our three-dimensional geometry model of the subducting Philippine Sea plate. Pale colors indicate areas through which no seismic rays passed. (b) Checkerboard test results and (c) traveltime fitting diagram for the entire profile. The vertical axis of (b) show the OBS numbers from north to south along the profile except for four OBSs for long-term observation.

Figure S13. First-arrival tomography results for profile NT04 off the Kii Peninsula: (a) First-arrival tomography based on the onshore–offshore seismic survey of the entire profile, including the landward extension in the onshore area. The horizontal axis indicates distance from the southern end of the offshore profile. The seismic reflectivity image obtained by the traveltime mapping method is superimposed in grayscale. The magenta line shows the plate interface interpreted from multichannel reflection data. Pale colors indicate areas through which no seismic rays passed. (b) Checkerboard test results and (c) traveltime fitting diagram for the OBS and densely deployed land station data and other onshore data along the entire profile. The velocity structure for distances from 0 to 270 km was analyzed by using airgun shot data

observed by OBSs and temporary land stations. The velocity structure beneath the onshore area from the distance of 270 km northward was analyzed by using onshore data, including from explosives. Airgun shot data recorded by three Hi-net stations along the landward extension of the profile were also used to constrain the onshore structure. The vertical axis of (c) show the OBS, land station and dynamite numbers from south to north along the profile.

Figure S14. First-arrival tomography results for profile NT06 off the Kii Peninsula: (a) First-arrival tomography results. The horizontal axis indicates distance from the southern end of the offshore profile. The seismic reflectivity image obtained by the traveltime mapping method is superimposed in grayscale. The blue line shows the plate interface interpreted from multichannel reflection data. Pale colors indicate areas through which no seismic rays passed. (b) Checkerboard test results and (c) traveltime fitting diagram for the entire profile. The vertical axis of (b) show the OBS numbers from north to south along the profile.

Figure S15. Verification of the three-dimensional model along profile HY02 in the Hyuga-nada region: (a) Differences between the three-dimensional model and the model obtained from our study (shown in Figure S4-2). (b) Traveltime fitting diagram for the three-dimensional model along the onshore–offshore profile. The horizontal axis indicates distance from the southern end of the profile. The vertical axis of (b) show the OBS and land station numbers from south to north along the profile.

Figure S16. Verification of the three-dimensional model along profile HY03 in the Hyuga-nada region: (a) Differences between the three-dimensional model and the model obtained from our study (shown in Figure S5-2). (b) Traveltime fitting diagram for the three-dimensional model along the profile. The horizontal axis indicates distance from the southwestern end of the profile. The vertical axis of (b) show the OBS numbers and southwest to northeast along the profile except for two OBSs located at the crosspoints with HY01 and HY02.

Figure S17. Verification of the three-dimensional model along profile HY04 in the Hyuga-nada region: (a) Differences between the three-dimensional model and the model obtained from our study (shown in Figure S6-2). (b) Traveltime fitting diagram for the three-dimensional model along the profile. The horizontal axis indicates distance from the southwestern end of the profile. The vertical axis of (b) show the OBS numbers and southwest to northeast along the profile except for two OBSs located at the crosspoints with HY01 and HY02.

Figure S18. Verification of the three-dimensional model along profile SK04 off Shikoku: (a) Differences between the three-dimensional model and the model obtained from our study (shown in Figure S7-2). (b) Traveltime fitting diagram for the three-dimensional model along the onshore–offshore profile. The horizontal axis indicates distance from the southern end of the profile. The vertical axis of (b) show the OBS and land station numbers from north to south along the profile except for two OBSs for long-term observation.

Figure S19. Verification of the three-dimensional model along profile TK02 off the Kii Channel: (a) Differences between the three-dimensional model and the model obtained from our study (shown in Figure S12). (b) Traveltime fitting diagram for the three-dimensional model along the profile. The horizontal axis indicates distance from the southern end of the offshore profile. The

difference in velocity is larger here than in the southwestern part of the study area because the velocities obtained from the first-arrival tomography were incorporated in the construction of the three-dimensional velocity model. In addition, the velocity information was too sparse for a reliable three-dimensional velocity model to be constructed. The vertical axis of (b) show the OBS numbers from north to south along the profile except for four OBSs for long-term observation.

Figure S20. Verification of the three-dimensional model along profile NT04 off the Kii Peninsula: (a) Differences between the three-dimensional model and the model obtained from our study (shown in Figure S12). (b) Traveltime fitting diagram for the three-dimensional model along the profile. The horizontal axis indicates distance from the southern end of the offshore profile. The difference in velocity is larger here than in the southwestern part of the study area because velocities obtained from the first-arrival tomography were incorporated in the construction of the three-dimensional velocity model and because the velocity information was too sparse for construction of a reliable three-dimensional velocity model. The vertical axis of (c) show the OBS, land station and dynamite numbers from south to north along the profile.

Figure S21. Verification of the three-dimensional model along profile NT06 off the Kii Peninsula: (a) Differences between the three-dimensional model and the model obtained from our study (shown in Figure S12). (b) Traveltime fitting diagram for the three-dimensional model along the profile. The horizontal axis indicates distance from the southern end of the offshore profile. The difference in velocity is larger here than in the southwestern part of the study area because velocities obtained from the first-arrival tomography were incorporated in the construction of the three-dimensional velocity model and because the velocity information was too sparse for construction of a reliable three-dimensional velocity model. The vertical axis of (b) show the OBS numbers from north to south along the profile.

SUPPLEMENTARY MATERIAL

Deviation of the Seismic Velocity Models Used for the Proposed Three-Dimensional Models

We used first-arrival tomography data to estimate seismic velocity models. The GeoCT-II software package, which is based on algorithms by Zhang et al. (1998) and Zhang and Toksöz (1998), was applied to all first-arrival data to ensure consistency of the analysis for seismic velocity models. Generally, we used a 0.1 km × 0.1 km grid for forward calculations and a 0.2 km × 0.2 km grid for inversion calculations. The inversion calculations were iterated until the root mean square of the traveltime residuals became smaller than the observed uncertainty (e.g., less than ±0.05 s; Figure S1). We also conducted checkerboard tests, using the method described by Zelt and Barton (1998), to estimate the spatial resolution of velocity anomalies. We assumed alternating anomalies of ±5% in the background velocity with a grid size of 7.5 km (horizontal) × 7.5 km or 15 km (vertical). The checkerboard patterns were recovered well in areas through which seismic rays corresponding to the traveltime data used for the traveltime tomography passed (e.g., Figure S1). In addition, we obtained seismic velocity models beneath onshore areas, along landward extensions of some offshore seismic profile lines, although these have relatively low resolution because there were only a few onshore Hi-net stations along the profiles, HY01, HY02, SK01 and SK04 (Figure 1).

We applied the reflection traveltime mapping method (TMM) (Fujie et al., 2006) to the wide-angle OBS data to obtain reflectivity images. Later arrivals of the prominent reflections were

picked with an uncertainty of ±0.1 s and mapped onto the velocity structure obtained by first-arrival refraction tomography. As a result, each later phase can be interpreted as having been reflected from several interfaces, such as the top of the oceanic crust and the oceanic Moho.

We then constructed a pseudolayer model based on the seismic velocity models and reflectivity images (Figure 2). In the pseudolayer model whom we call so, reflectors with velocity jumps are indicated by thin (approximately 500 m thick) layers with large velocity gradients. We then calculated theoretical traveltime curves and iteratively modified the model parameters until all of the picked observed data along the seismic profile could be explained consistently. The iteration was continued until the differences between the observed and calculated traveltimes became less than approximately ±0.1 s for both first and later arrivals. We used a two-dimensional ray-tracing technique (Zelt and Smith, 1992) for traveltime calculations. The pseudolayer model was determined mainly by a trial-and-error approach and by taking account of the geological interpretation for the geometry of the subducting Philippine Sea plate based on the previous studies (e.g., Kodaira et al., 2000; Takahashi et al., 2002). Finally, after finalizing the reflectors within the pseudolayer model, we again applied first-arrival tomography to the velocity model to confirm the traveltime fitting of the first arrivals. Because of the geological interpretation for the geometry of the subducting plate, some of the traveltime residuals for the first arrivals became larger than those numerically analyzed from the first-arrival tomography, as shown in Figure S1. Nevertheless, the theoretical first and later traveltimes calculated from the pseudolayer model can be explained by traveltime residuals of less than ±0.1 s with few exceptions. The errors in the positions of reflectors with a thickness of 500 m were estimated by multiplying the picked traveltime uncertainties (< ±0.1 s) by the average velocity above the reflectors. In this study, the error in the reflector positions was always less than 800 m because the average velocity above the reflector never exceeded 8.0 km/s (Figure S2). All velocity structure models and traveltime fitting diagrams used in this study are shown in Figures 2 and S3–S14.

REFERENCES CITED IN THE SUPPLEMENTARY MATERIAL

Fujie, G., Ito, A., Kodaira, S., Takahashi, N., and Kaneda, Y., 2006, Confirming sharp bending of the Pacific plate in the northern Japan trench subduction zone by applying a traveltime mapping method: Physics of the Earth and Planetary Interiors, v. 167, p. 72–85, doi:10.1016/j.pepi.2006.03.013.

Kodaira, S., Takahashi, N., Park, J.O., Mochizuki, K., Shinohara, M., and Kimura, S., 2000, The western Nankai Trough seismogenic zone: Result from wide-angle Ocean Bottom Seismographic Survey, Journal of Geophysical Research, v. 105, p. 5887-5905.

Takahashi, N., Kodaira, S., Nakanishi, A., Park, J.O., Miura, S., Tsuru, T., Kaneda, Y., Suyehiro, K., Hirata, N., and Iwasaki, T., 2002, Seismic structure of the western end of the Nankai Trough seismogenic zone, v. 107, ESE2, doi: 10.1029/2000JB000121

Zhang, J., and Toksöz, M.N., 1998, Nonlinear refraction traveltime tomography: Geophysics, v. 63, p. 1726–1737, doi:10.1190/1.1444468.

Zhang, J., ten Brink, U.S., and Toksöz, M.N., 1998, Nonlinear refraction and reflection travel time tomography: Journal of Geophysical Research, v. 103, p. 29,743–29,757, doi:10.1029/98JB01981.

Zelt, C.A., and Barton, P.J., 1998, Three-dimensional seismic refraction tomography: A comparison of two methods applied to data from the Faroe Basin: Journal of Geophysical Research, v. 103, p. 7187–7210.

Zelt, C.A., and Smith, R.B., 1998, Seismic travel time inversion for 2-D crustal velocity structure: Geophysical Journal International, v. 108, p. 16–31.

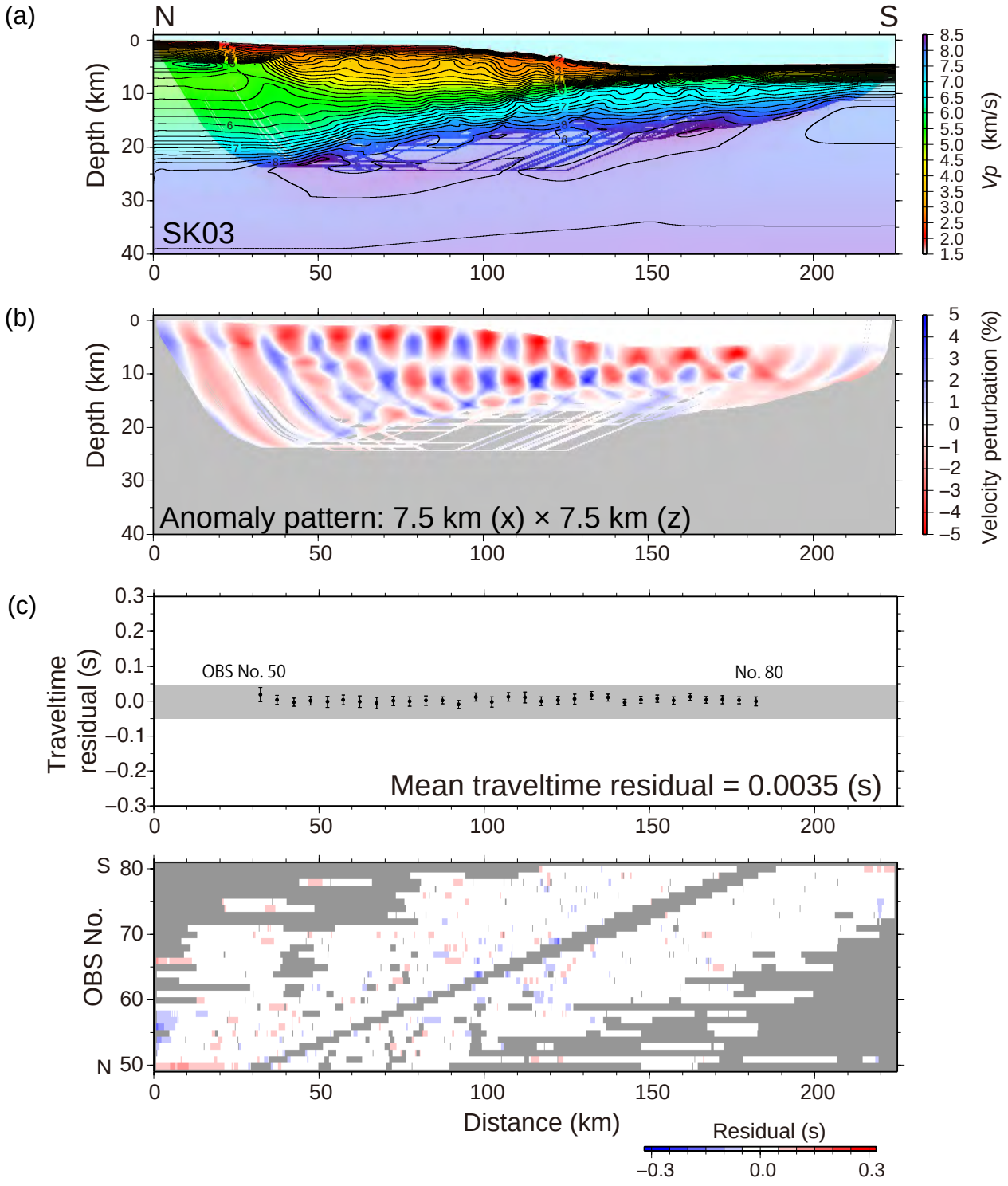
(a)
N
S
Depth (km)
SK03
Vp (km/s)
(b)
Depth (km)
Anomaly pattern: 7.5 km (x) × 7.5 km (z)
Velocity perturbation (%)
(c)
Traveltime residual (s)
OBS No. 50
No. 80
Mean traveltime residual = 0.0035 (s)
OBS No.
S
N
Distance (km)
Residual (s)

Figure S1

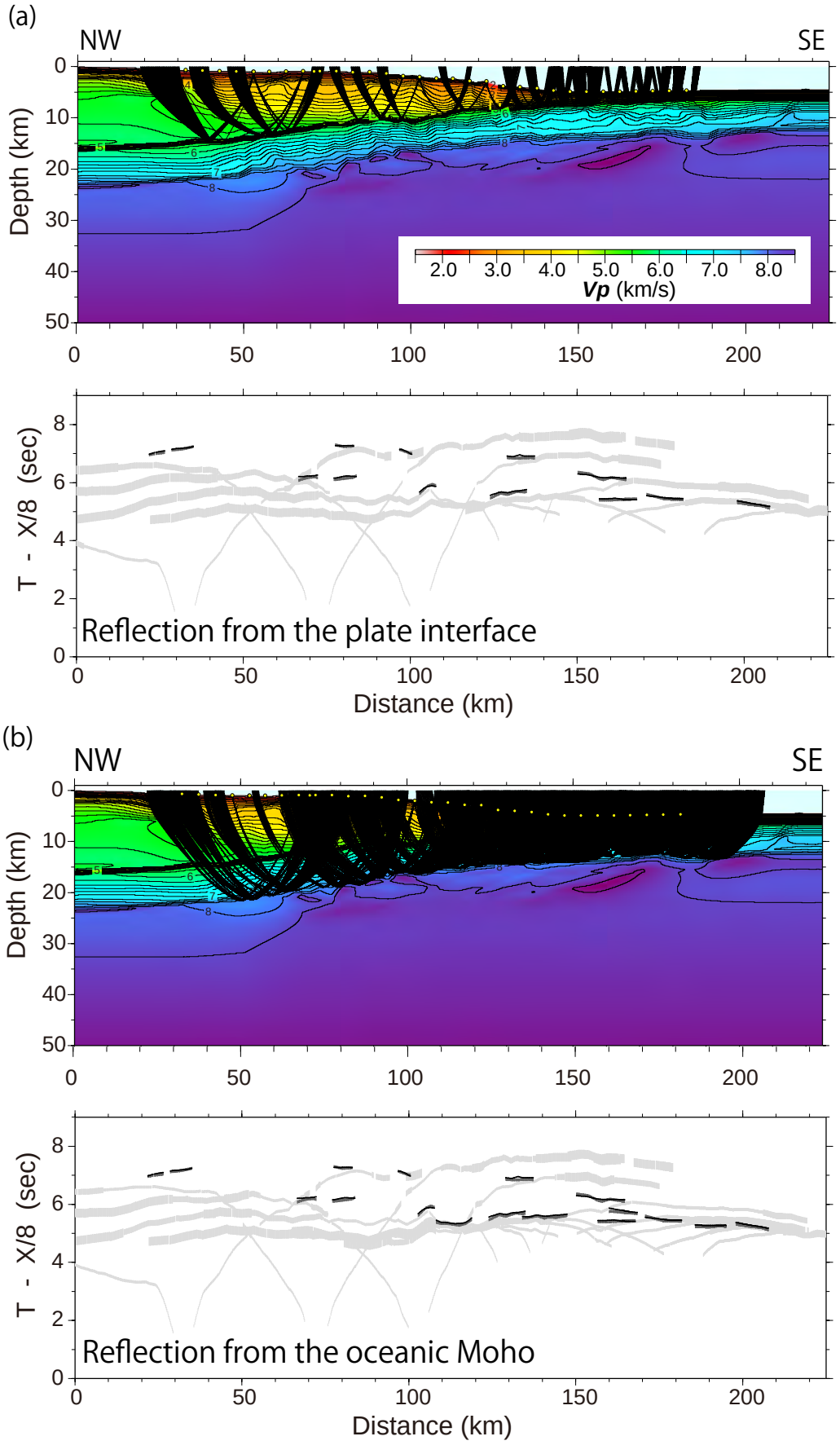
(a)
NW
SE
Depth (km)
0
10
20
30
40
50
0
50
100
150
200
2.0
3.0
4.0
5.0
6.0
7.0
8.0
Vp (km/s)
T - X/8 (sec)
0
2
4
6
8
Reflection from the plate interface
Distance (km)
(b)
NW
SE
Depth (km)
T - X/8 (sec)
Reflection from the oceanic Moho
Distance (km)

Figure S2

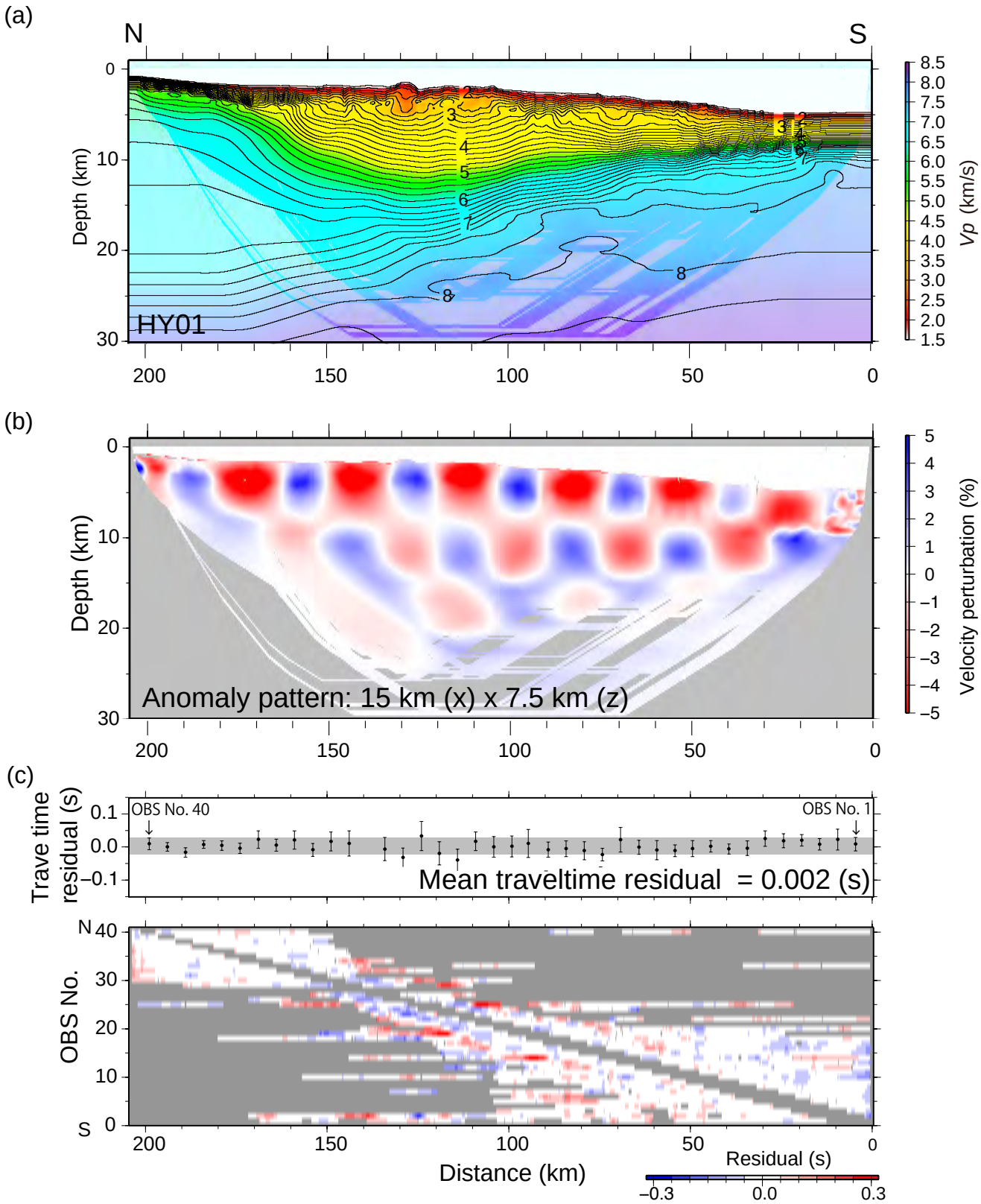
(a)
N
S
Depth (km)
HY01
Vp (km/s)
(b)
Depth (km)
Anomaly pattern: 15 km (x) x 7.5 km (z)
Velocity perturbation (%)
(c)
Trave time residual (s)
OBS No. 40
OBS No. 1
Mean traveltime residual = 0.002 (s)
OBS No.
Distance (km)
Residual (s)

Figure S3-1

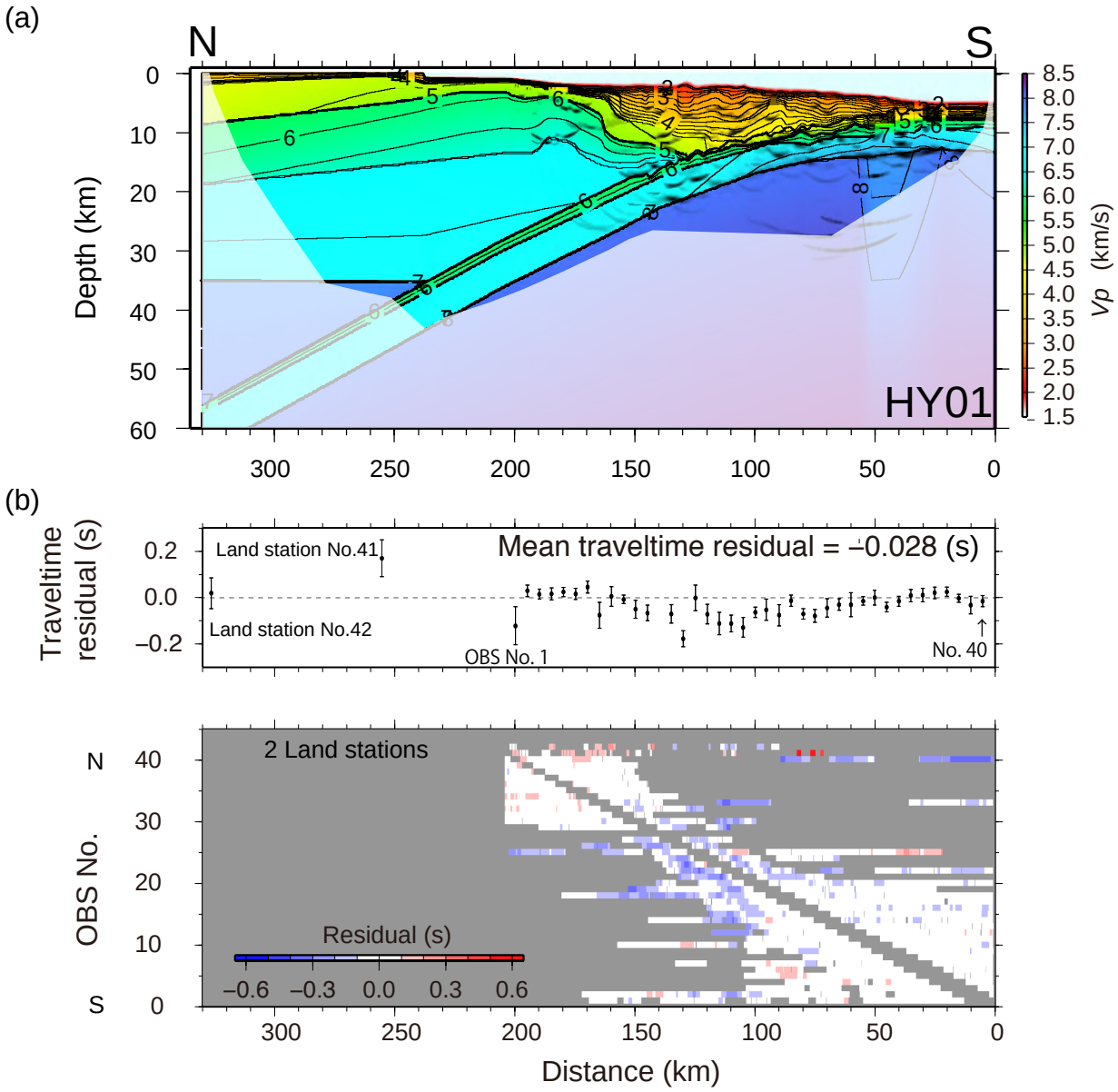
(a)
N
S
HY01
Depth (km)
Vp (km/s)
(b)
Traveltime residual (s)
Land station No.41
Land station No.42
Mean traveltime residual = −0.028 (s)
OBS No. 1
No. 40
2 Land stations
OBS No.
Residual (s)
Distance (km)

Figure S3-2

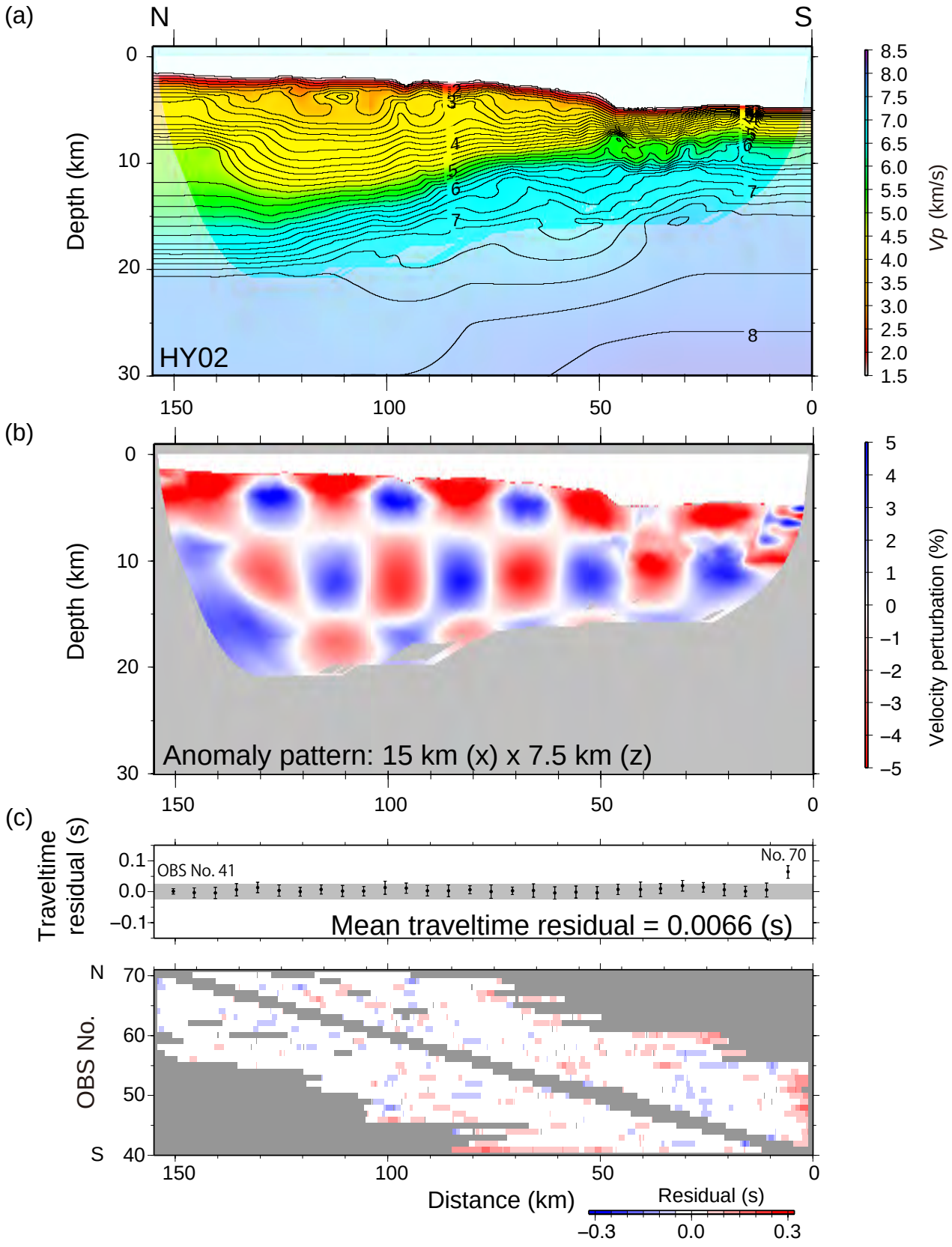
(a)
N
S
Depth (km)
HY02
Vp (km/s)
(b)
Anomaly pattern: 15 km (x) x 7.5 km (z)
Velocity perturbation (%)
(c)
Traveltime residual (s)
OBS No. 41
No. 70
Mean traveltime residual = 0.0066 (s)
OBS No.
Distance (km)
Residual (s)

Figure S4-1

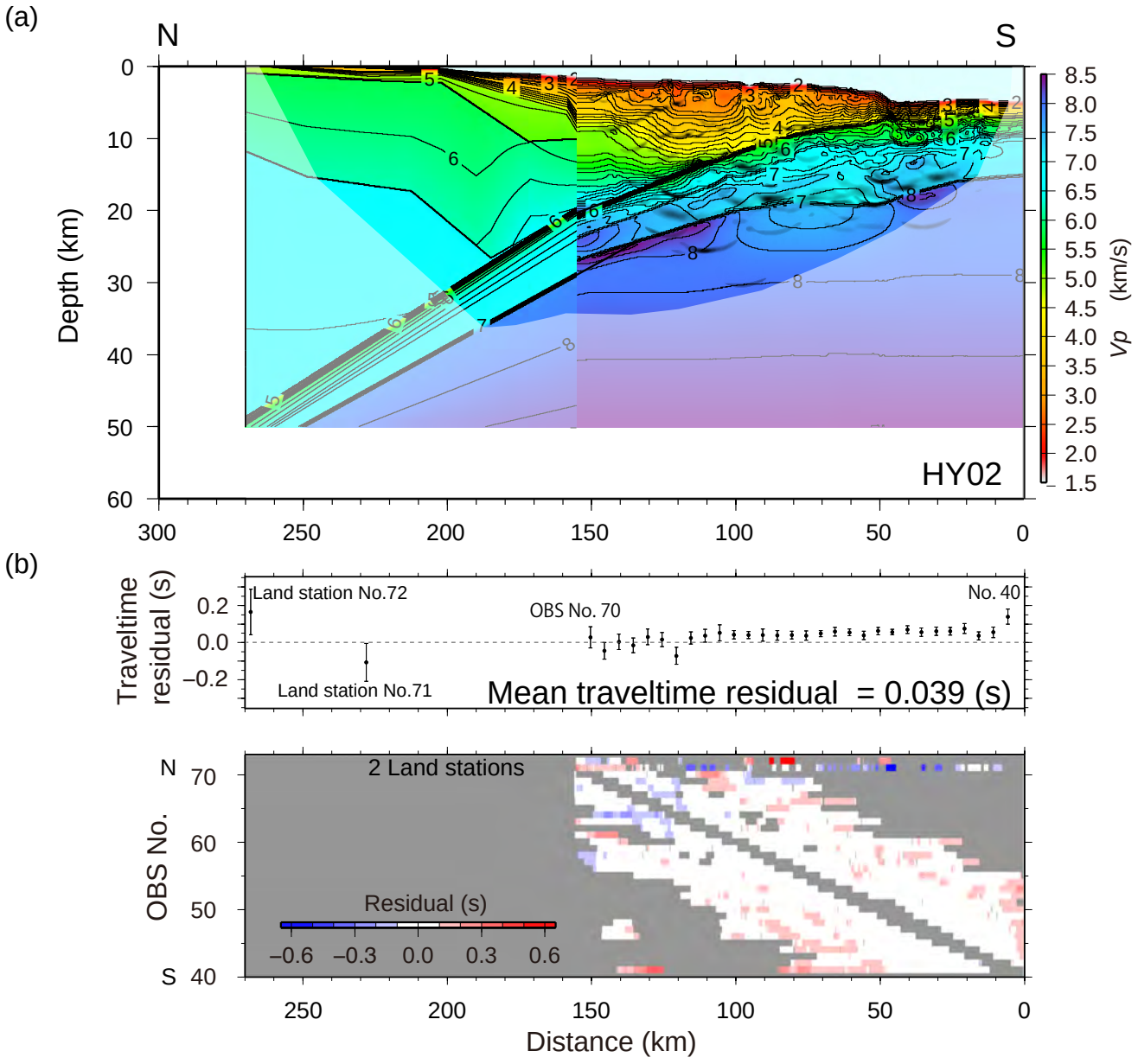
(a)
N
S
Depth (km)
HY02
Vp (km/s)
(b)
Traveltime residual (s)
Land station No.72
OBS No. 70
No. 40
Land station No.71
Mean traveltime residual = 0.039 (s)
2 Land stations
OBS No.
Residual (s)
Distance (km)

Figure S4-2

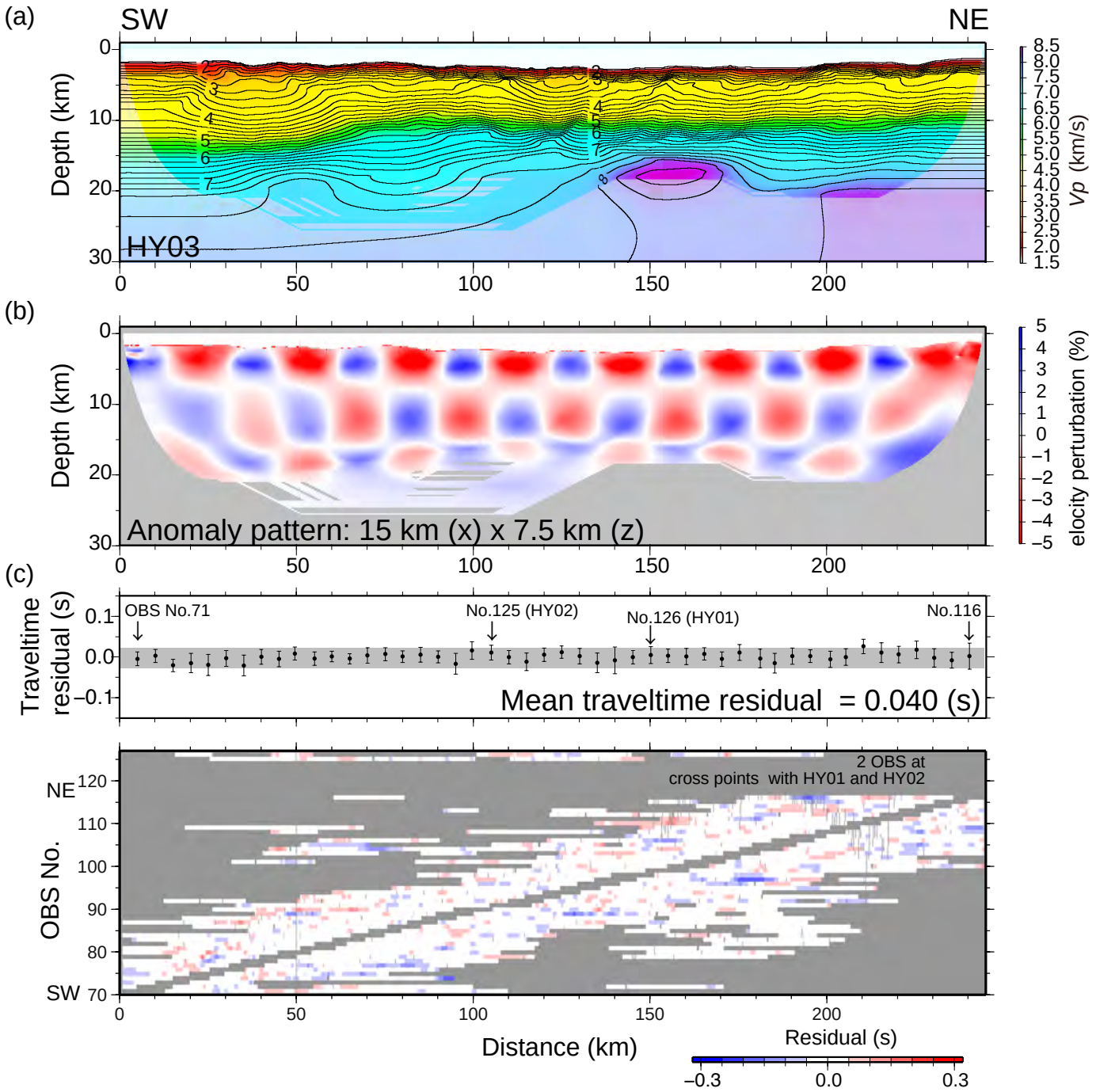
(a)
SW
NE
Depth (km)
HY03
Vp (km/s)
(b)
Depth (km)
Anomaly pattern: 15 km (x) x 7.5 km (z)
elocity perturbation (%)
(c)
Traveltime residual (s)
OBS No.71
No.125 (HY02)
No.126 (HY01)
No.116
Mean traveltime residual = 0.040 (s)
2 OBS at
cross points with HY01 and HY02
NE
SW
OBS No.
Distance (km)
Residual (s)

Figure S5-1

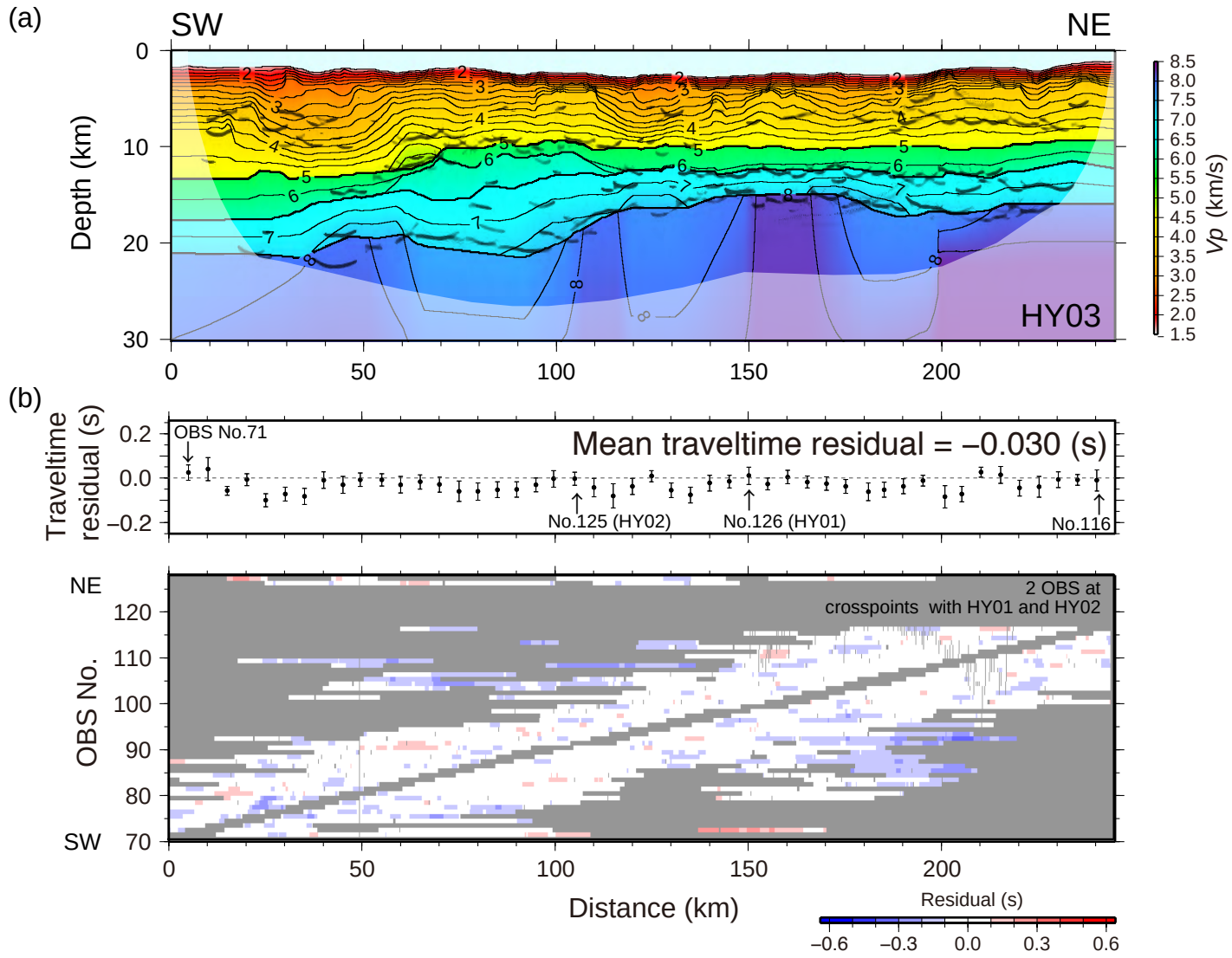
(a)
SW
NE
Depth (km)
HY03
Vp (km/s)
(b)
Traveltime residual (s)
OBS No.71
Mean traveltime residual = −0.030 (s)
No.125 (HY02)
No.126 (HY01)
No.116
OBS No.
2 OBS at
crosspoints with HY01 and HY02
Distance (km)
Residual (s)

Figure S5-2

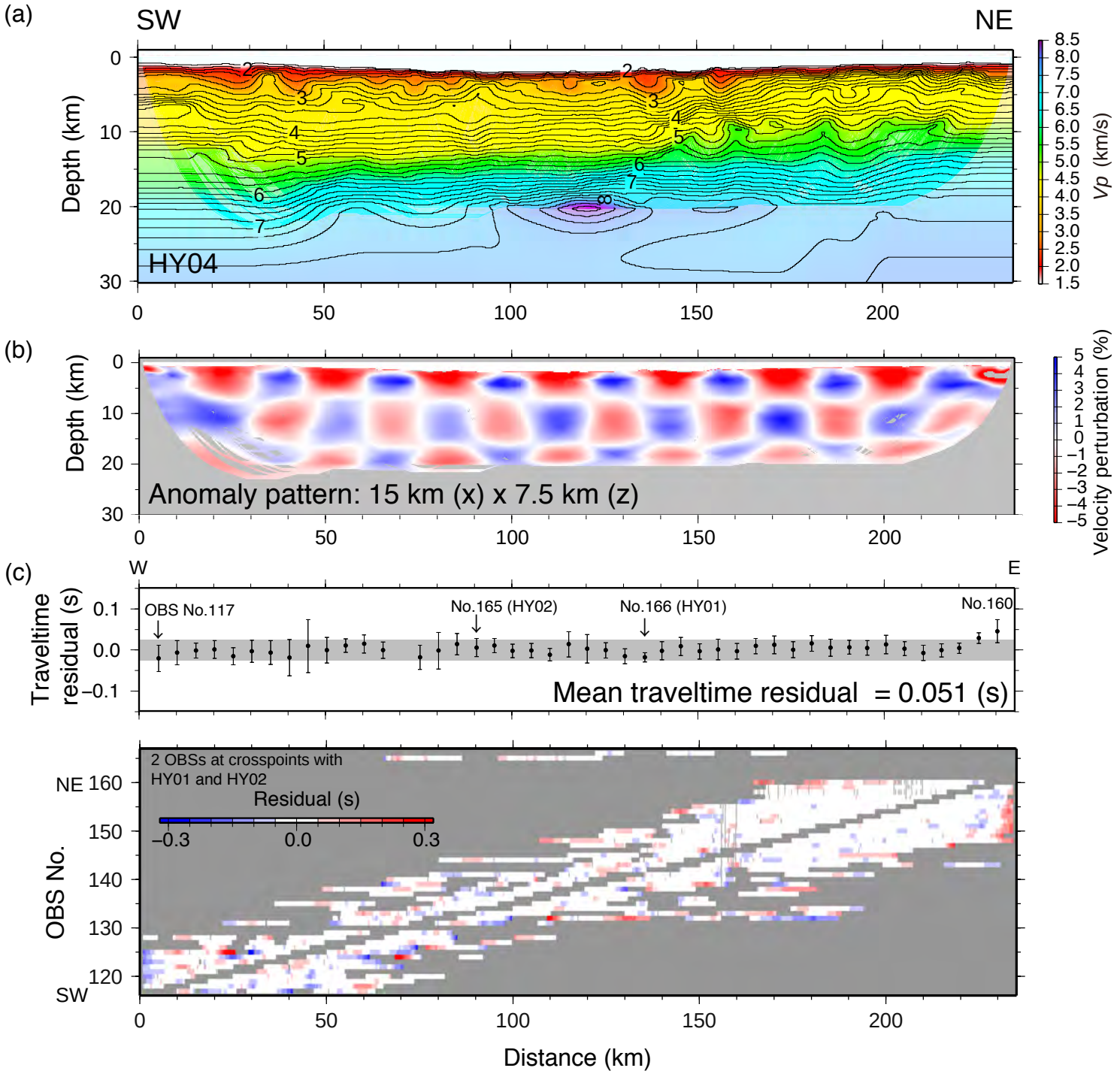
(a)
SW
NE
Depth (km)
HY04
Vp (km/s)
(b)
Anomaly pattern: 15 km (x) x 7.5 km (z)
Velocity perturbation (%)
(c)
W
E
Traveltime residual (s)
OBS No.117
No.165 (HY02)
No.166 (HY01)
No.160
Mean traveltime residual = 0.051 (s)
2 OBSs at crosspoints with HY01 and HY02
Residual (s)
OBS No.
Distance (km)

Figure S6-1

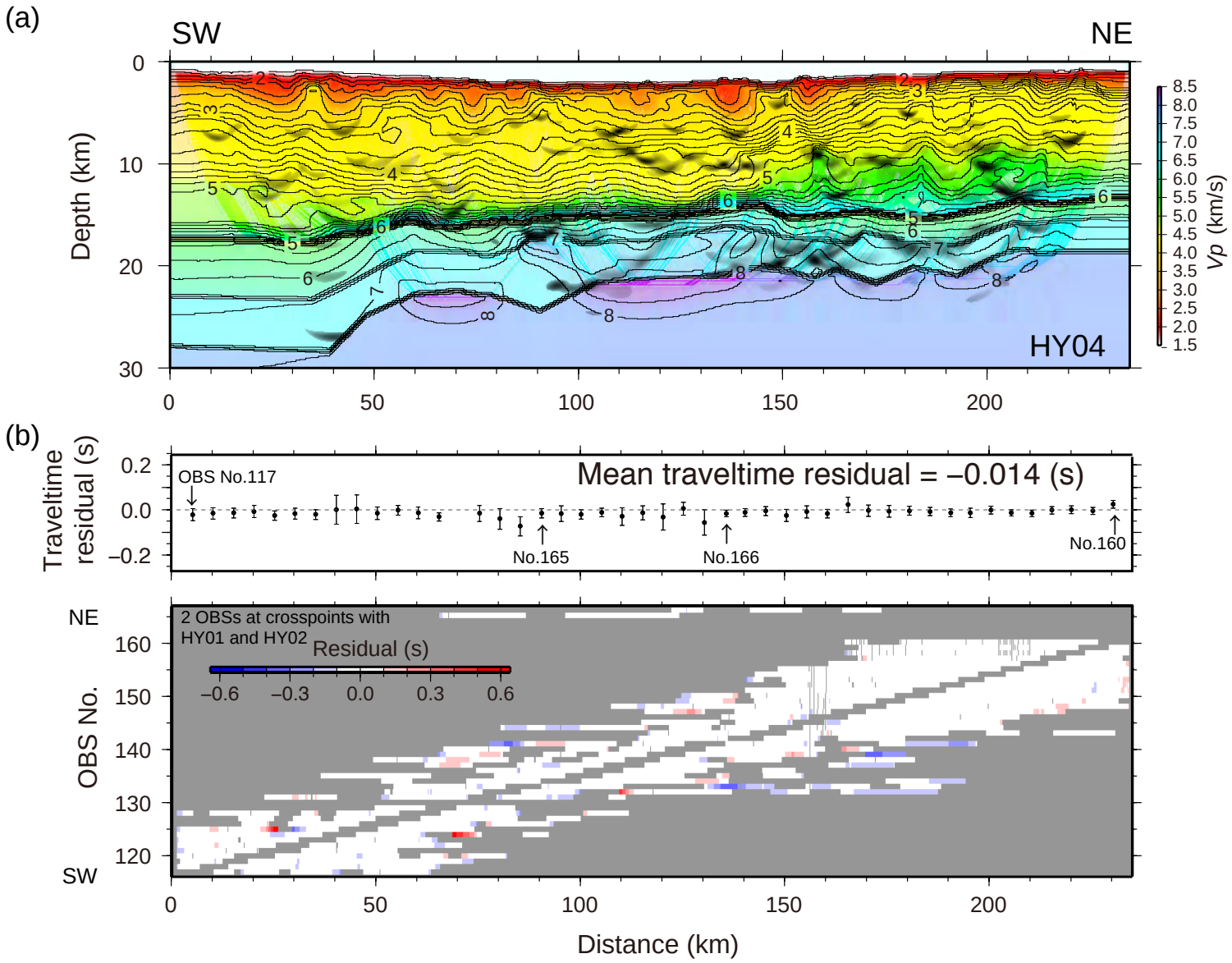
(a)
SW
NE
Depth (km)
HY04
Vp (km/s)
(b)
Traveltime residual (s)
OBS No.117
Mean traveltime residual = –0.014 (s)
No.165
No.166
No.160
2 OBSs at crosspoints with HY01 and HY02
Residual (s)
OBS No.
Distance (km)

Figure S6-2

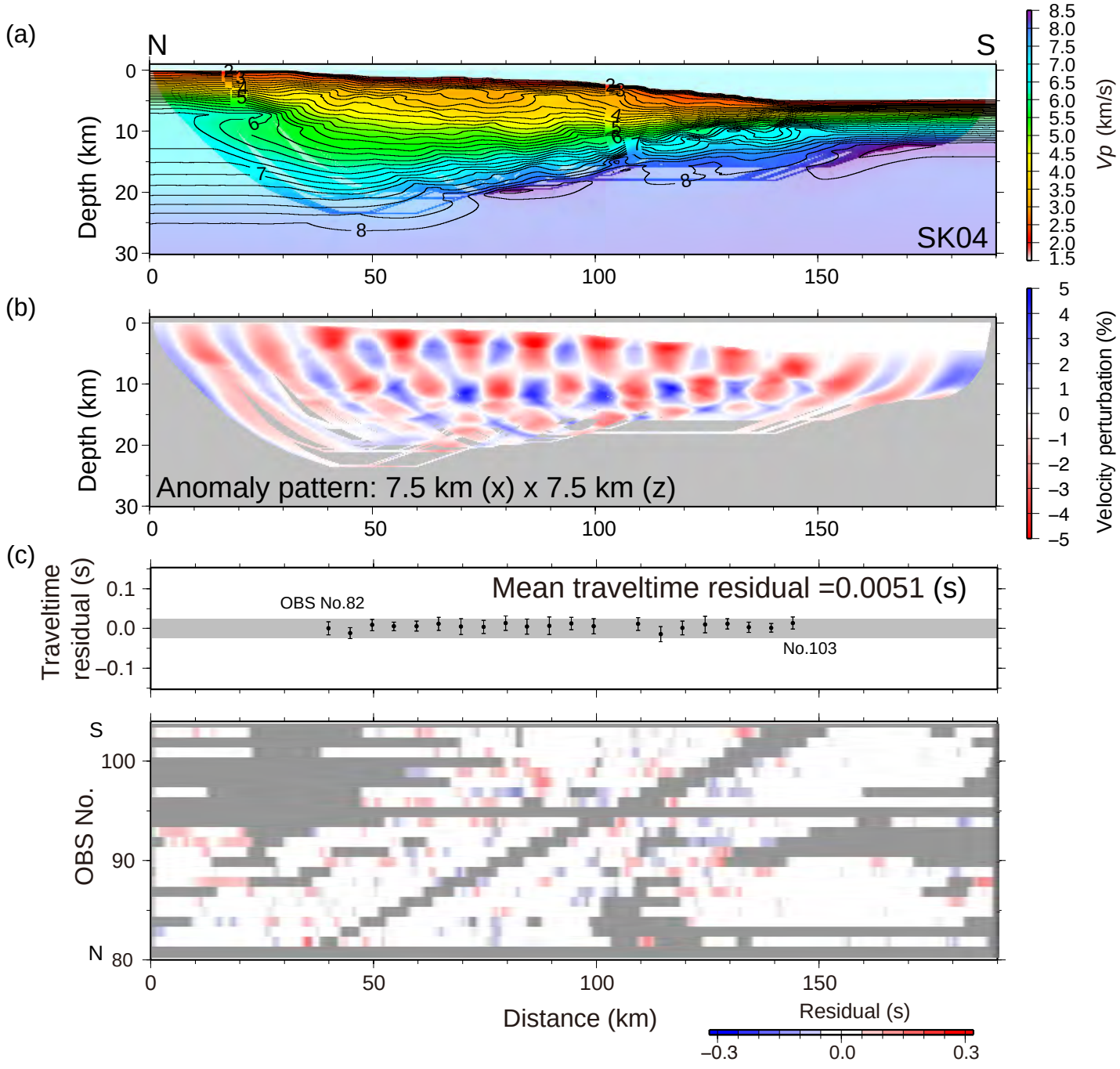
(a)
N
S
Depth (km)
SK04
Vp (km/s)
(b)
Anomaly pattern: 7.5 km (x) x 7.5 km (z)
Velocity perturbation (%)
(c)
Traveltime residual (s)
Mean traveltime residual =0.0051 (s)
OBS No.82
No.103
OBS No.
Distance (km)
Residual (s)

Figure S7-1

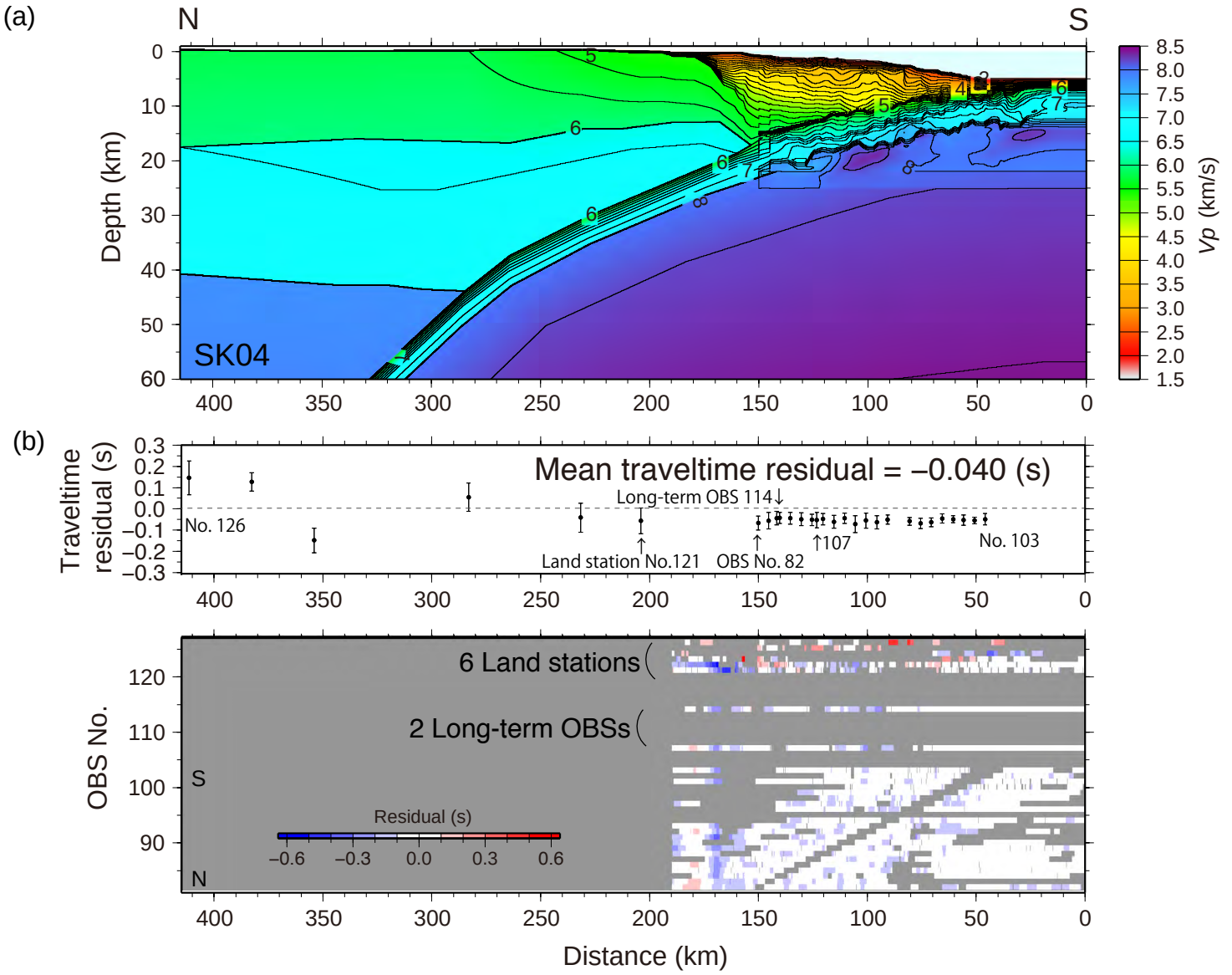
(a)
N
S
Depth (km)
SK04
Vp (km/s)
(b)
Traveltime residual (s)
Mean traveltime residual = –0.040 (s)
Long-term OBS 114
No. 126
Land station No.121
OBS No. 82
107
No. 103
6 Land stations
2 Long-term OBSs
OBS No.
S
N
Residual (s)
–0.6
–0.3
0.0
0.3
0.6
Distance (km)

Figure S7-2

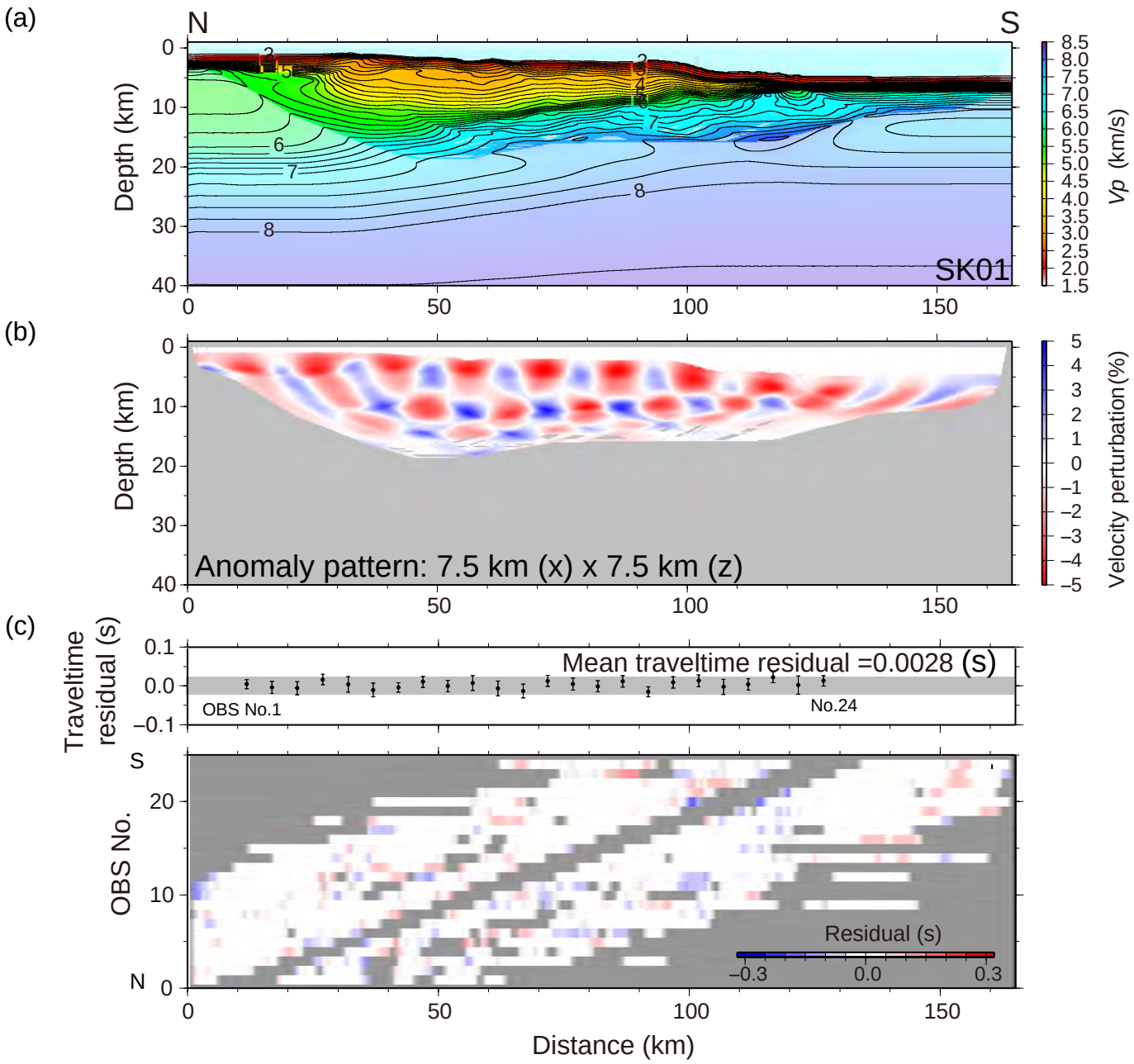
(a)
N
S
Depth (km)
SK01
Vp (km/s)
(b)
Depth (km)
Anomaly pattern: 7.5 km (x) x 7.5 km (z)
Velocity perturbation (%)
(c)
Traveltime residual (s)
Mean traveltime residual =0.0028 (s)
OBS No.1
No.24
OBS No.
S
N
Residual (s)
Distance (km)

Figure S8-1

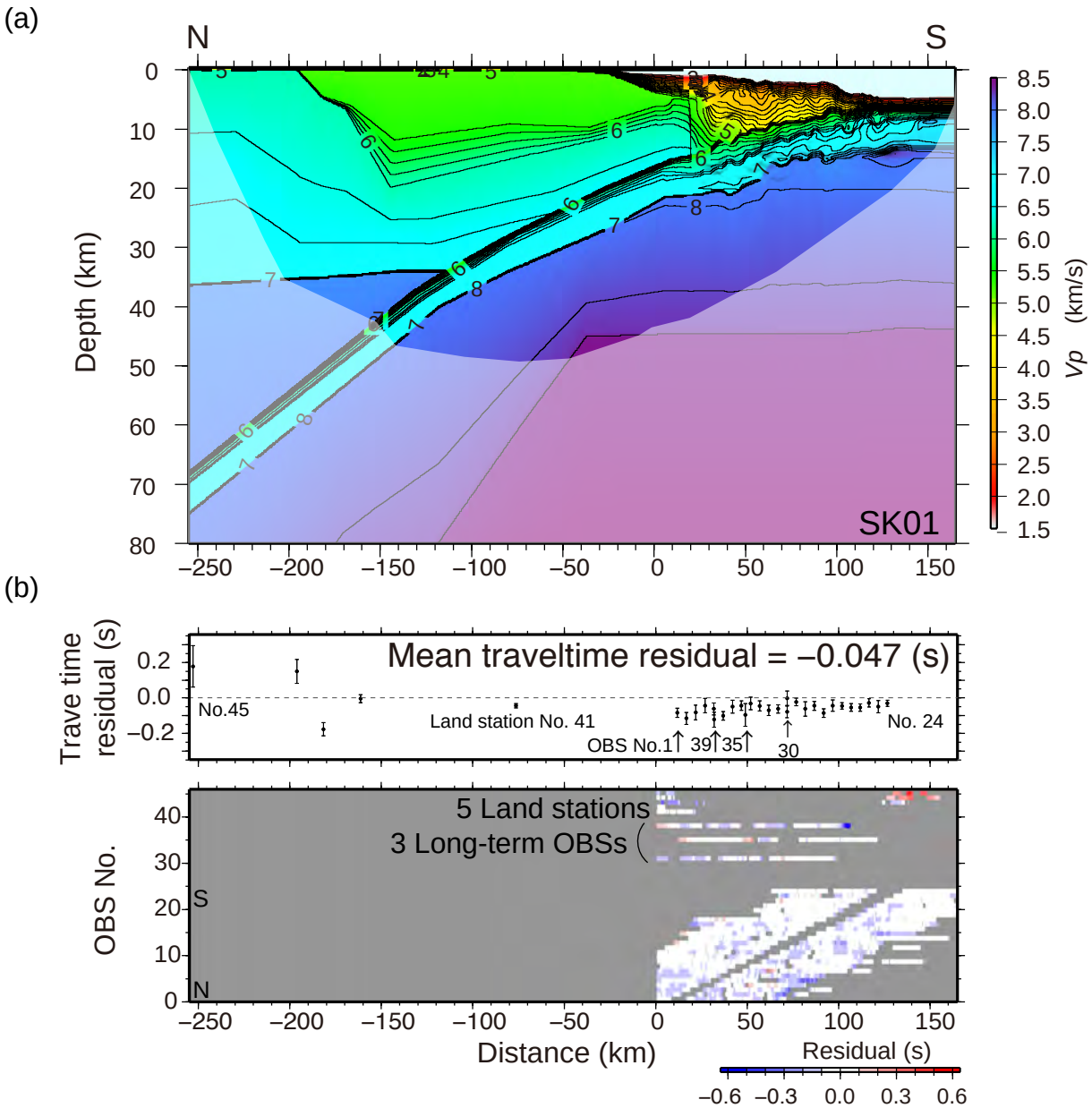
(a)
N
S
Depth (km)
SK01
Vp (km/s)
(b)
Trave time residual (s)
Mean traveltime residual = –0.047 (s)
No.45
Land station No. 41
No. 24
OBS No.1
39
35
30
OBS No.
5 Land stations
3 Long-term OBSs
S
N
Distance (km)
Residual (s)

Figure S8-2

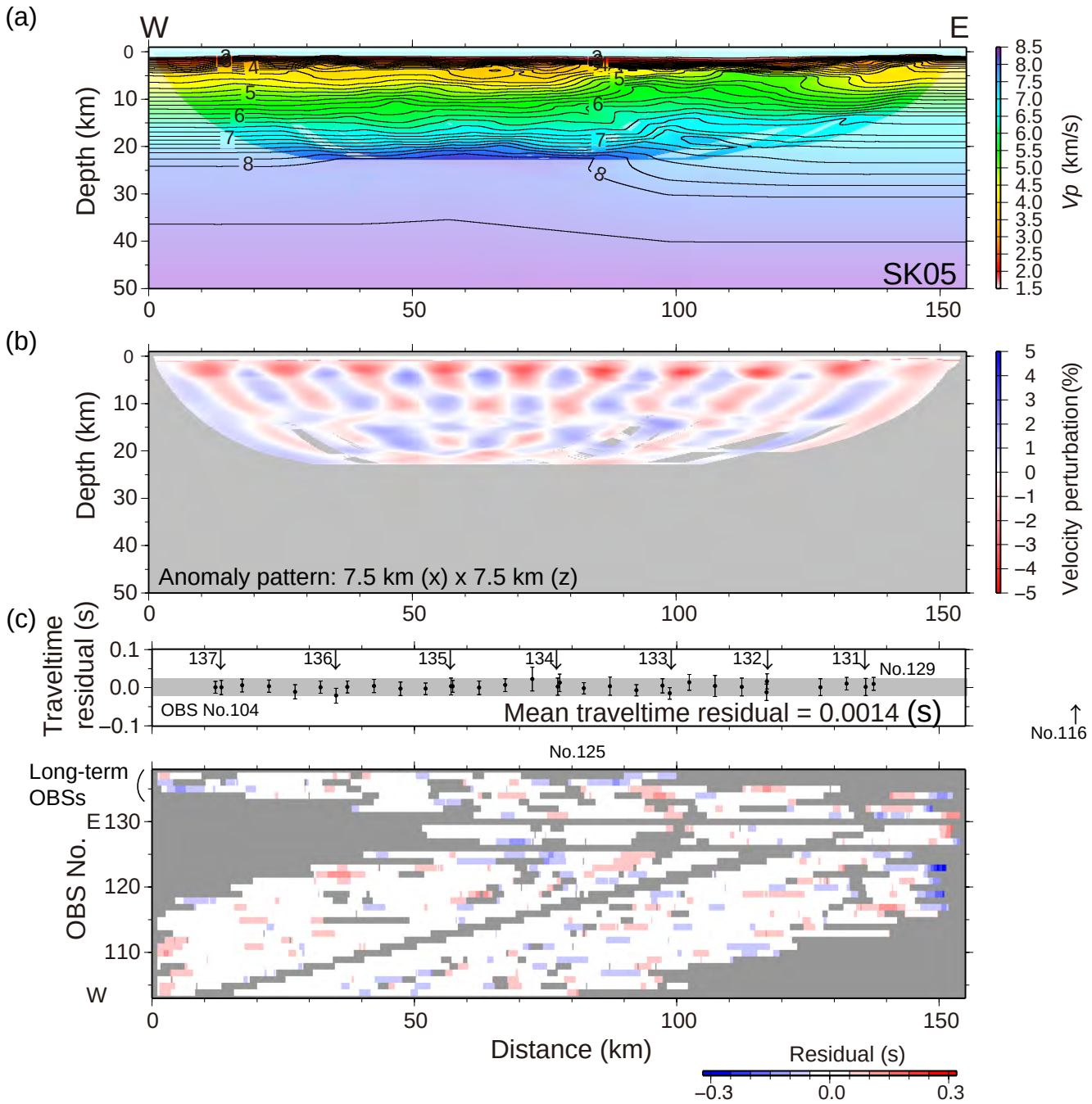
(a)
W
E
Depth (km)
SK05
Vp (km/s)
(b)
Anomaly pattern: 7.5 km (x) x 7.5 km (z)
Velocity perturbation (%)
(c)
Traveltime residual (s)
OBS No.104
Mean traveltime residual = 0.0014 (s)
No.129
No.116
No.125
Long-term OBSs
OBS No.
Distance (km)
Residual (s)

Figure S9-1

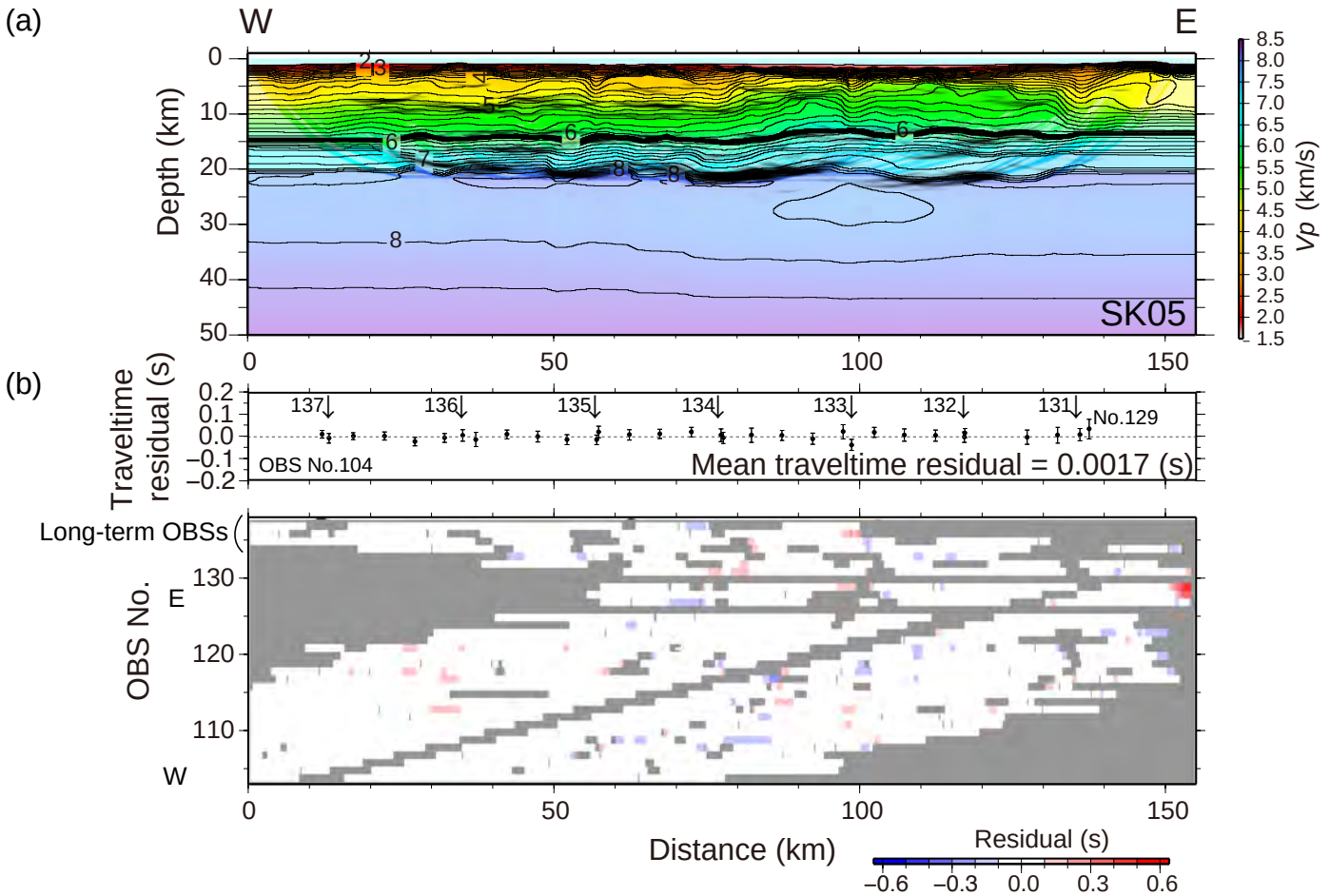
(a)
W
E
Depth (km)
SK05
Vp (km/s)
(b)
Traveltime residual (s)
OBS No.104
No.129
Mean traveltime residual = 0.0017 (s)
Long-term OBSs
OBS No.
Distance (km)
Residual (s)

Figure S9-2

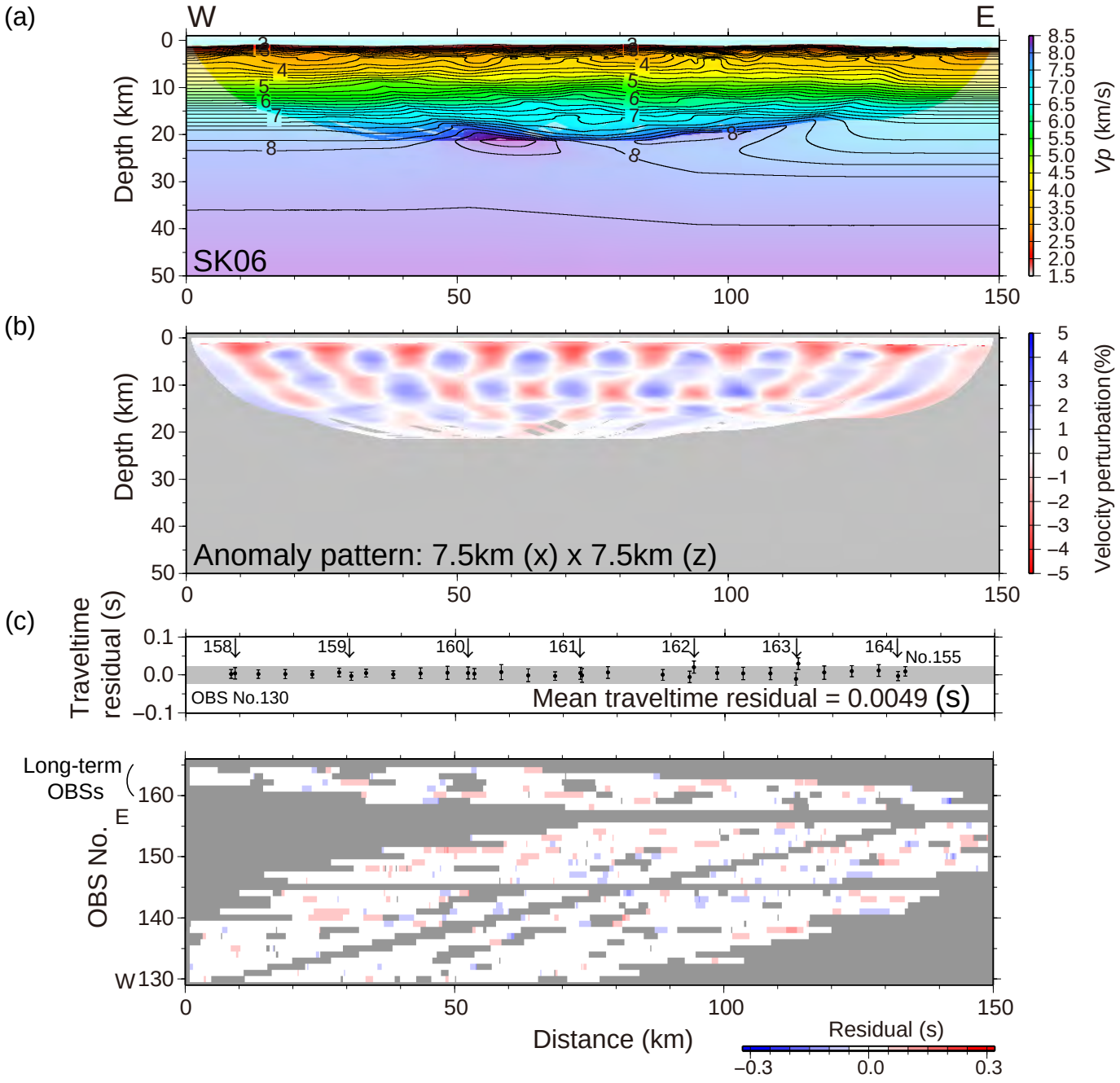
(a)
W
E
Depth (km)
SK06
Vp (km/s)
(b)
Depth (km)
Anomaly pattern: 7.5km (x) x 7.5km (z)
Velocity perturbation (%)
(c)
Traveltime residual (s)
158
159
160
161
162
163
164
No.155
OBS No.130
Mean traveltime residual = 0.0049 (s)
Long-term OBSs
OBS No.
E
W
Distance (km)
Residual (s)

Figure S10-1

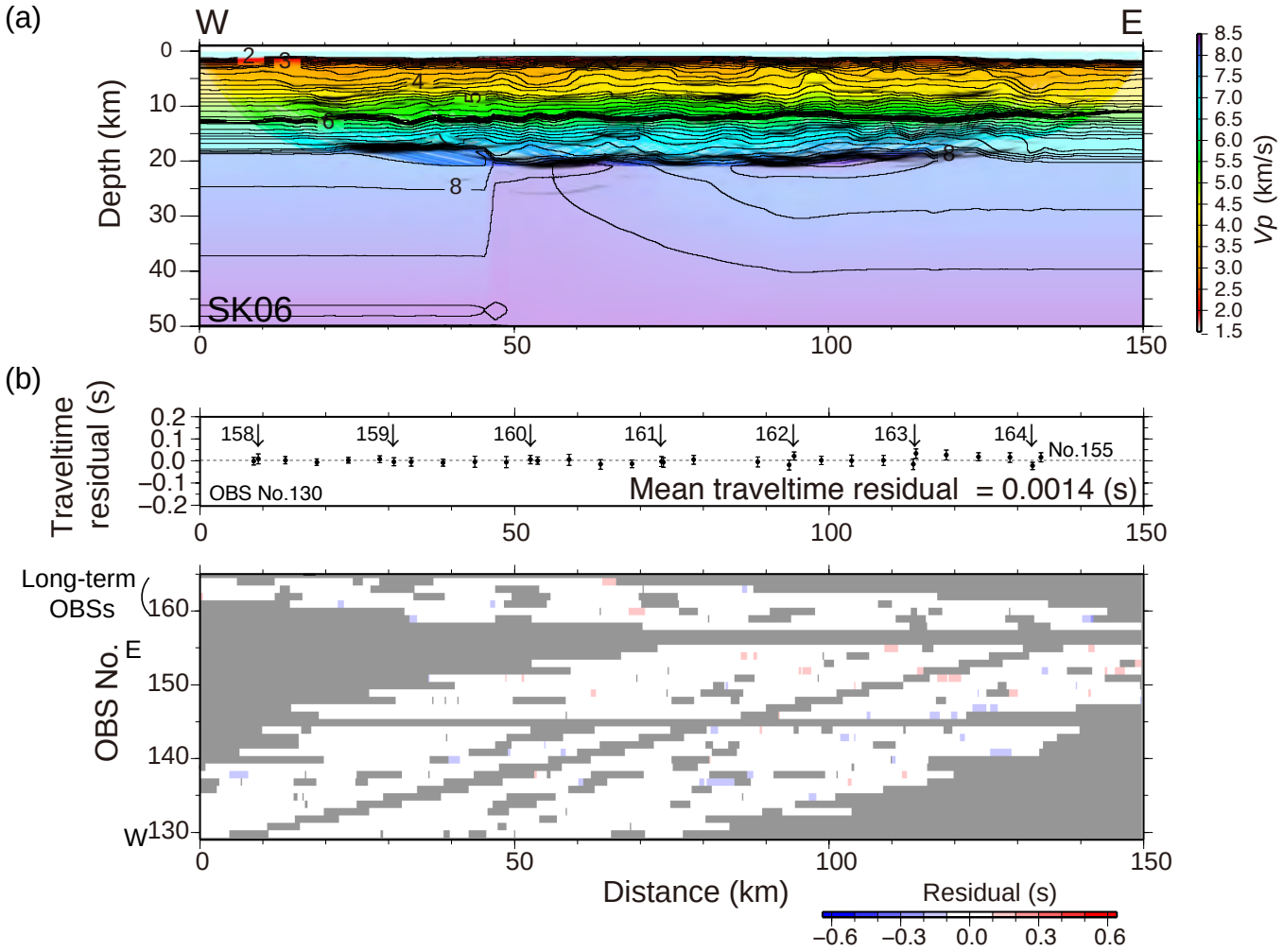
(a)
W
E
Depth (km)
SK06
Vp (km/s)
(b)
Traveltime residual (s)
OBS No.130
No.155
Mean traveltime residual = 0.0014 (s)
Long-term OBSs
OBS No.
Distance (km)
Residual (s)

Figure S10-2

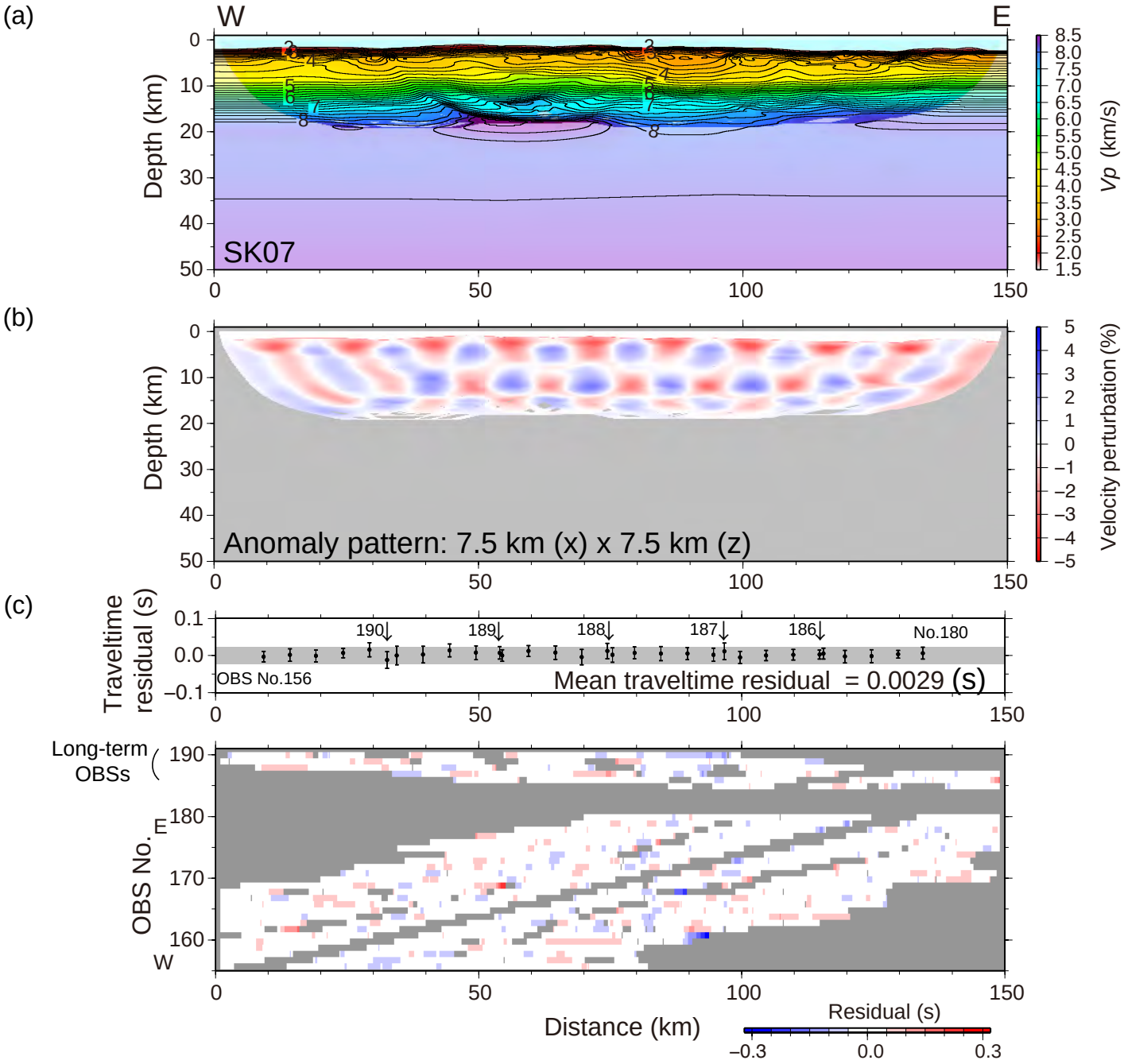
(a)
W
E
Depth (km)
SK07
Vp (km/s)
(b)
Depth (km)
Anomaly pattern: 7.5 km (x) x 7.5 km (z)
Velocity perturbation (%)
(c)
Traveltime residual (s)
190
189
188
187
186
No.180
OBS No.156
Mean traveltime residual = 0.0029 (s)
Long-term OBSs
OBS No.
E
W
Distance (km)
Residual (s)

Figure S11-1

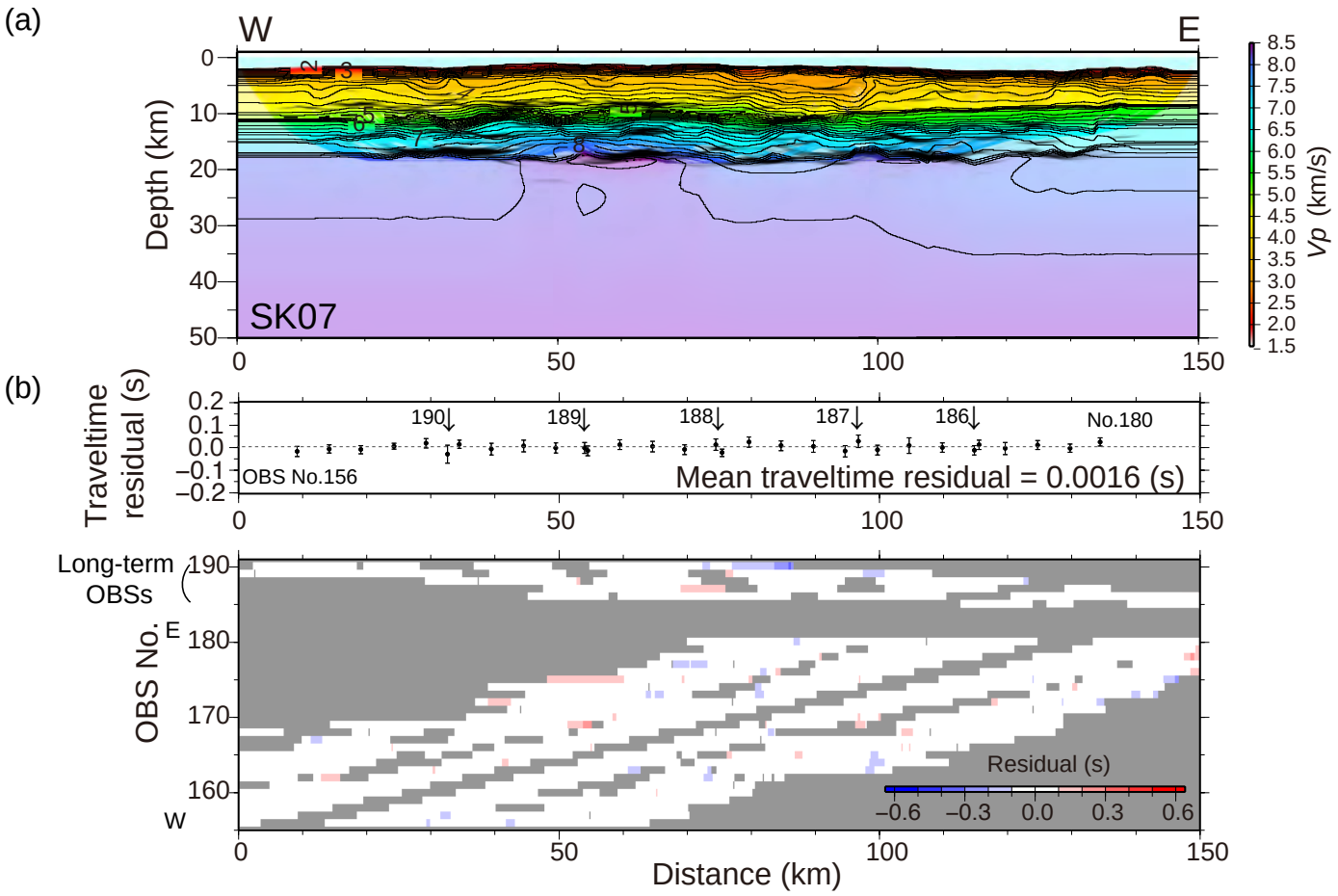
(a)
W
E
Depth (km)
SK07
Vp (km/s)
(b)
Traveltime residual (s)
OBS No.156
No.180
Mean traveltime residual = 0.0016 (s)
Long-term OBSs
OBS No.
E
W
Residual (s)
Distance (km)

Figure S11-2

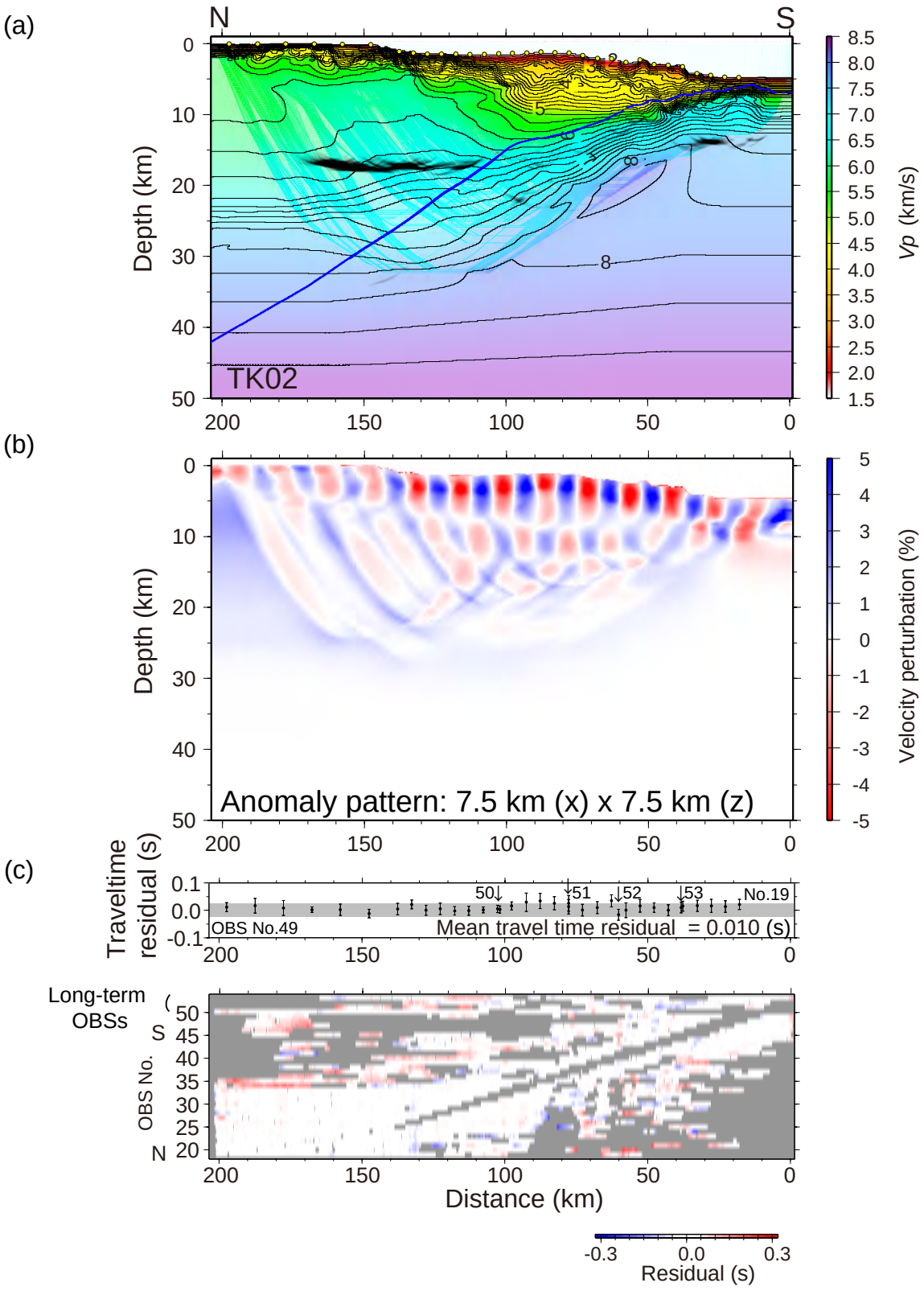
(a)
N
S
Depth (km)
TK02
Vp (km/s)
(b)
Depth (km)
Anomaly pattern: 7.5 km (x) x 7.5 km (z)
Velocity perturbation (%)
(c)
Traveltime residual (s)
OBS No.49
Mean travel time residual = 0.010 (s)
No.19
Long-term OBSs
OBS No.
S
N
Distance (km)
Residual (s)

Figure S12

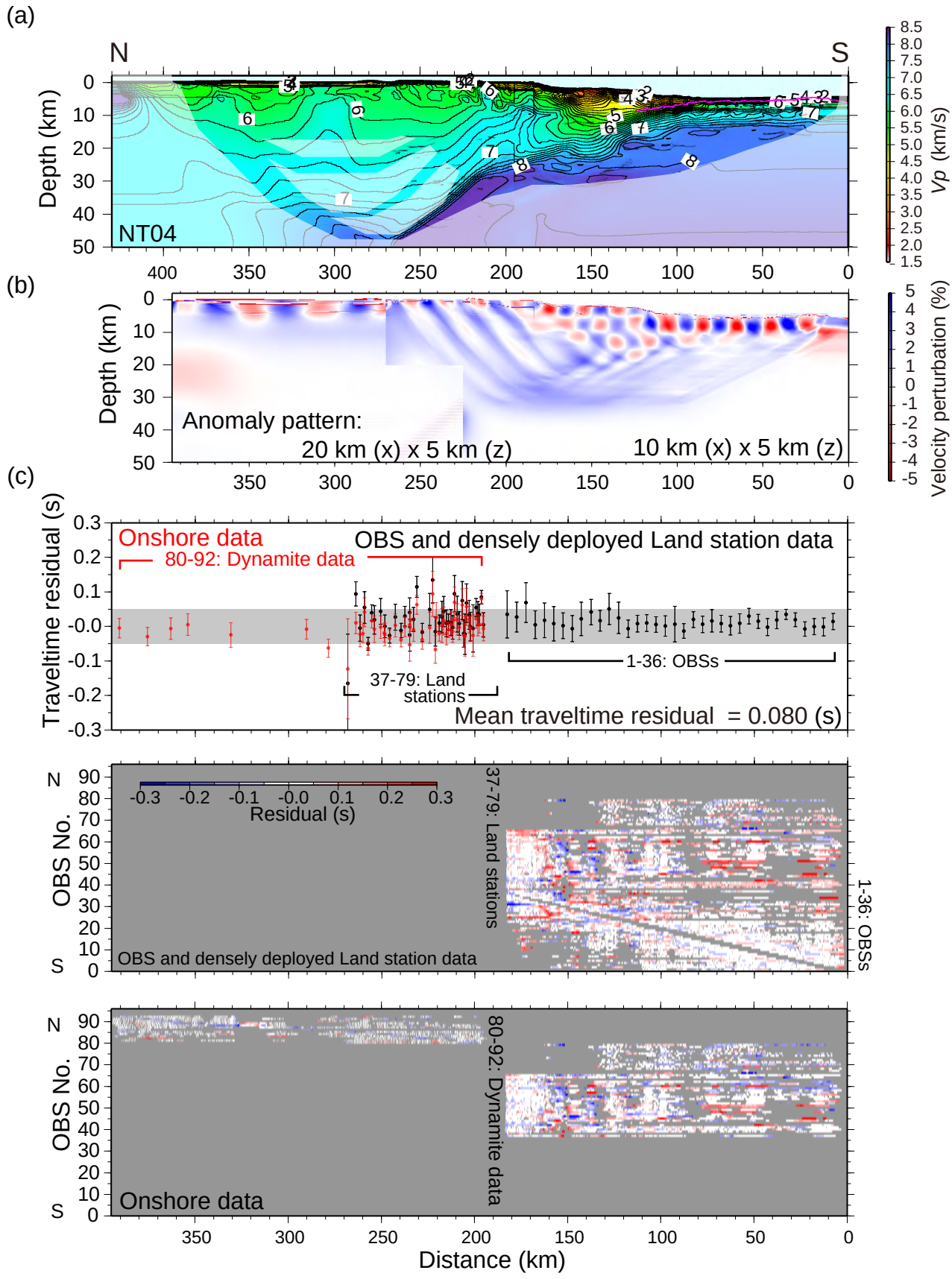
(a)
N
S
Depth (km)
NT04
Vp (km/s)
(b)
Anomaly pattern:
20 km (x) x 5 km (z)
10 km (x) x 5 km (z)
Velocity perturbation (%)
(c)
Traveltime residual (s)
Onshore data
80-92: Dynamite data
OBS and densely deployed Land station data
1-36: OBSs
37-79: Land stations
Mean traveltime residual = 0.080 (s)
OBS No.
Residual (s)
37-79: Land stations
1-36: OBSs
OBS and densely deployed Land station data
80-92: Dynamite data
Onshore data
Distance (km)

Figure S13

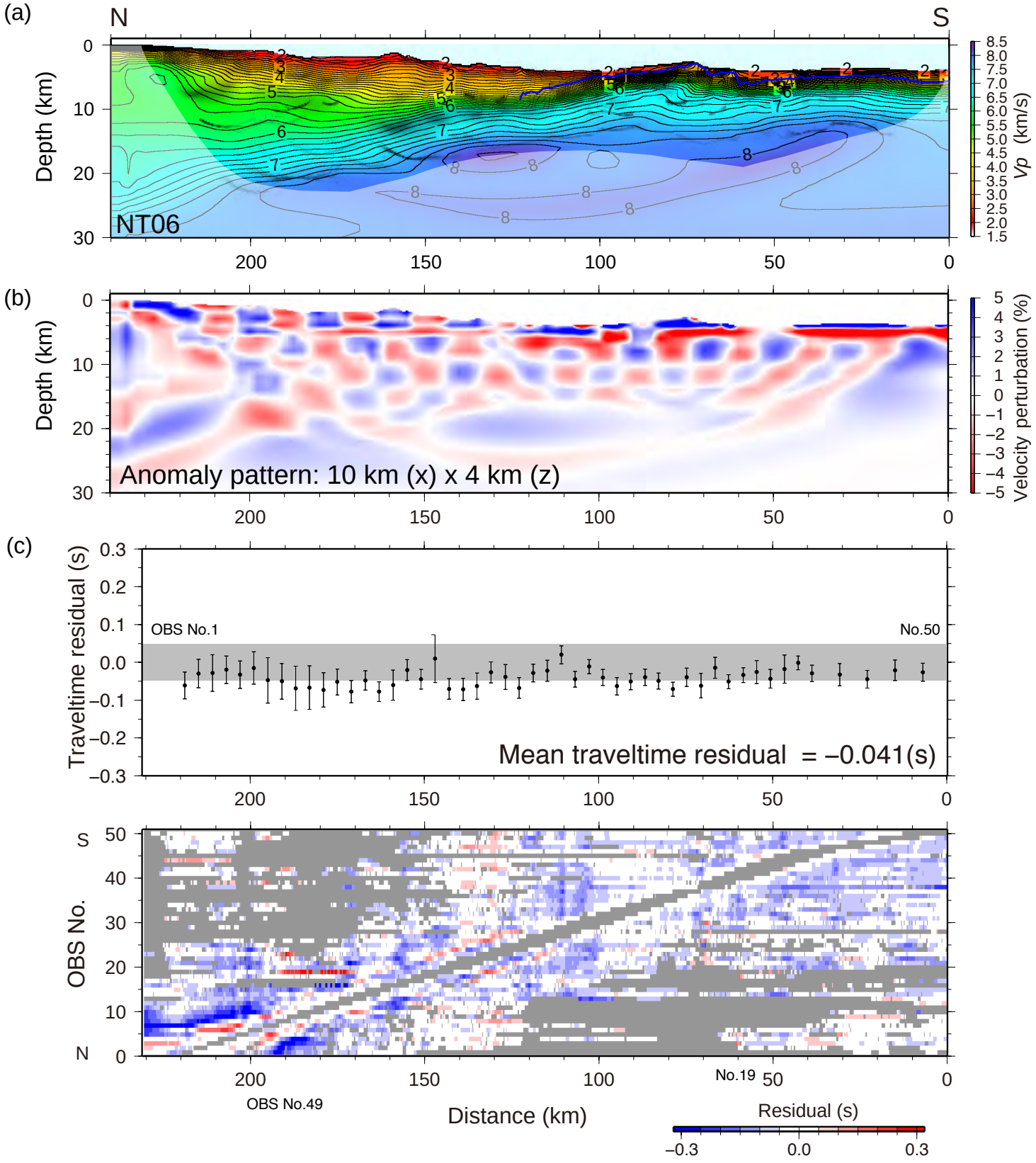
(a)
N
S
Depth (km)
NT06
Vp (km/s)
(b)
Depth (km)
Anomaly pattern: 10 km (x) x 4 km (z)
Velocity perturbation (%)
(c)
Traveltime residual (s)
OBS No.1
No.50
Mean traveltime residual = −0.041(s)
OBS No.
S
N
OBS No.49
No.19
Distance (km)
Residual (s)

Figure S14

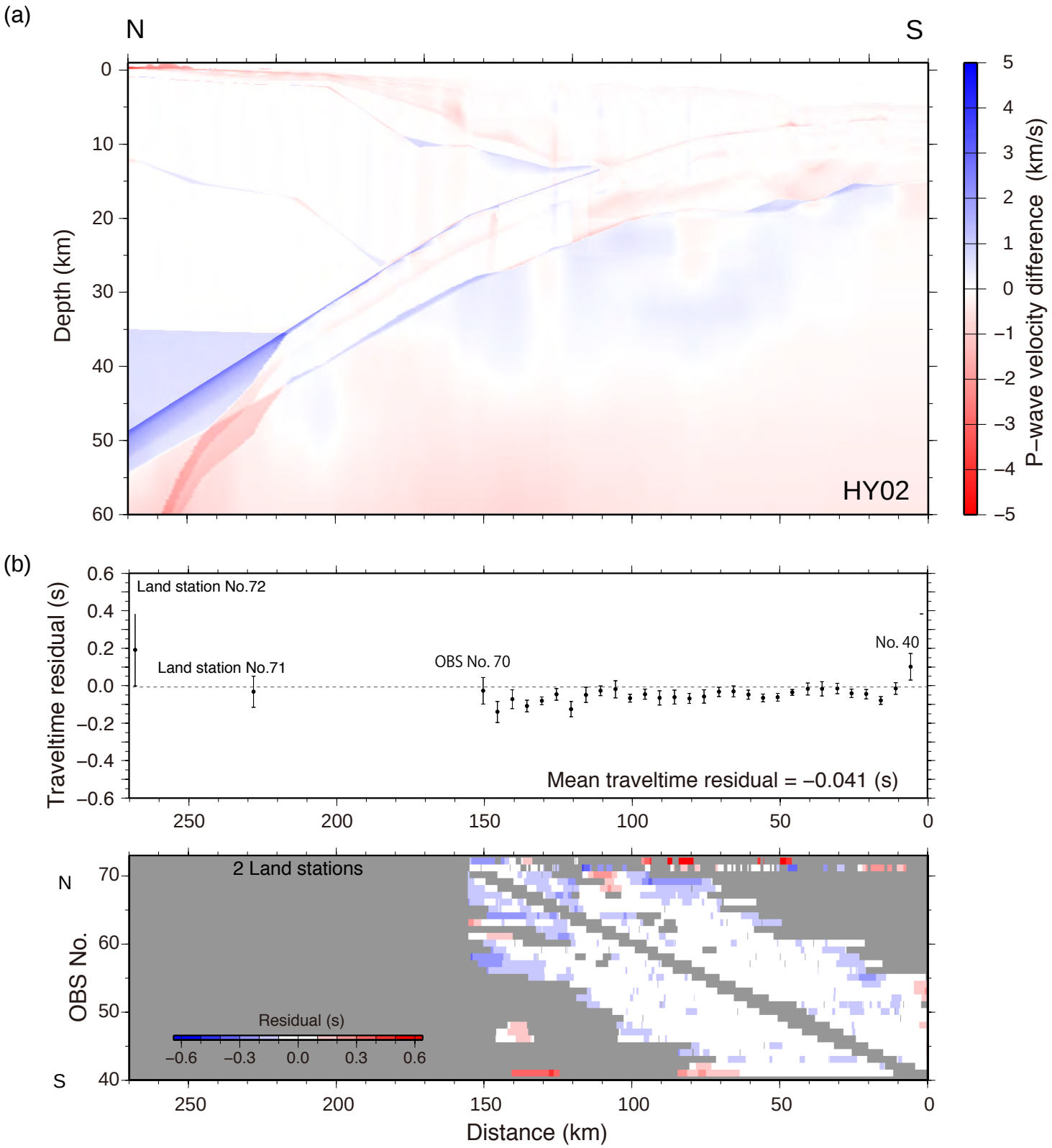
(a)
N
S
Depth (km)
HY02
P–wave velocity difference (km/s)
(b)
Traveltime residual (s)
Land station No.72
Land station No.71
OBS No. 70
No. 40
Mean traveltime residual = –0.041 (s)
2 Land stations
OBS No.
Residual (s)
Distance (km)

Figure S15

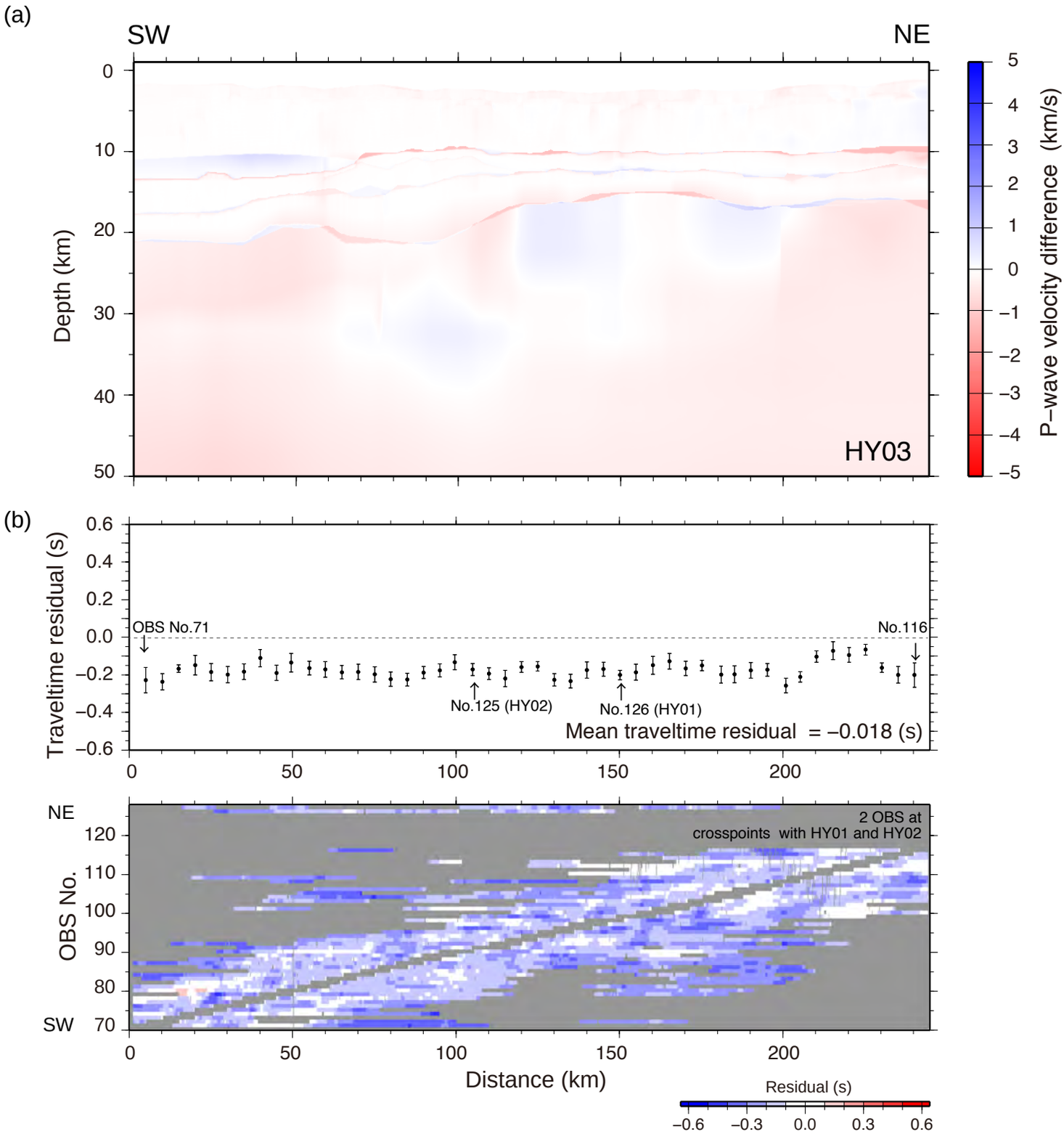
(a)
SW
NE
Depth (km)
HY03
P−wave velocity difference (km/s)
(b)
Traveltime residual (s)
OBS No.71
No.116
No.125 (HY02)
No.126 (HY01)
Mean traveltime residual = −0.018 (s)
OBS No.
2 OBS at
crosspoints with HY01 and HY02
Distance (km)
Residual (s)

Figure S16

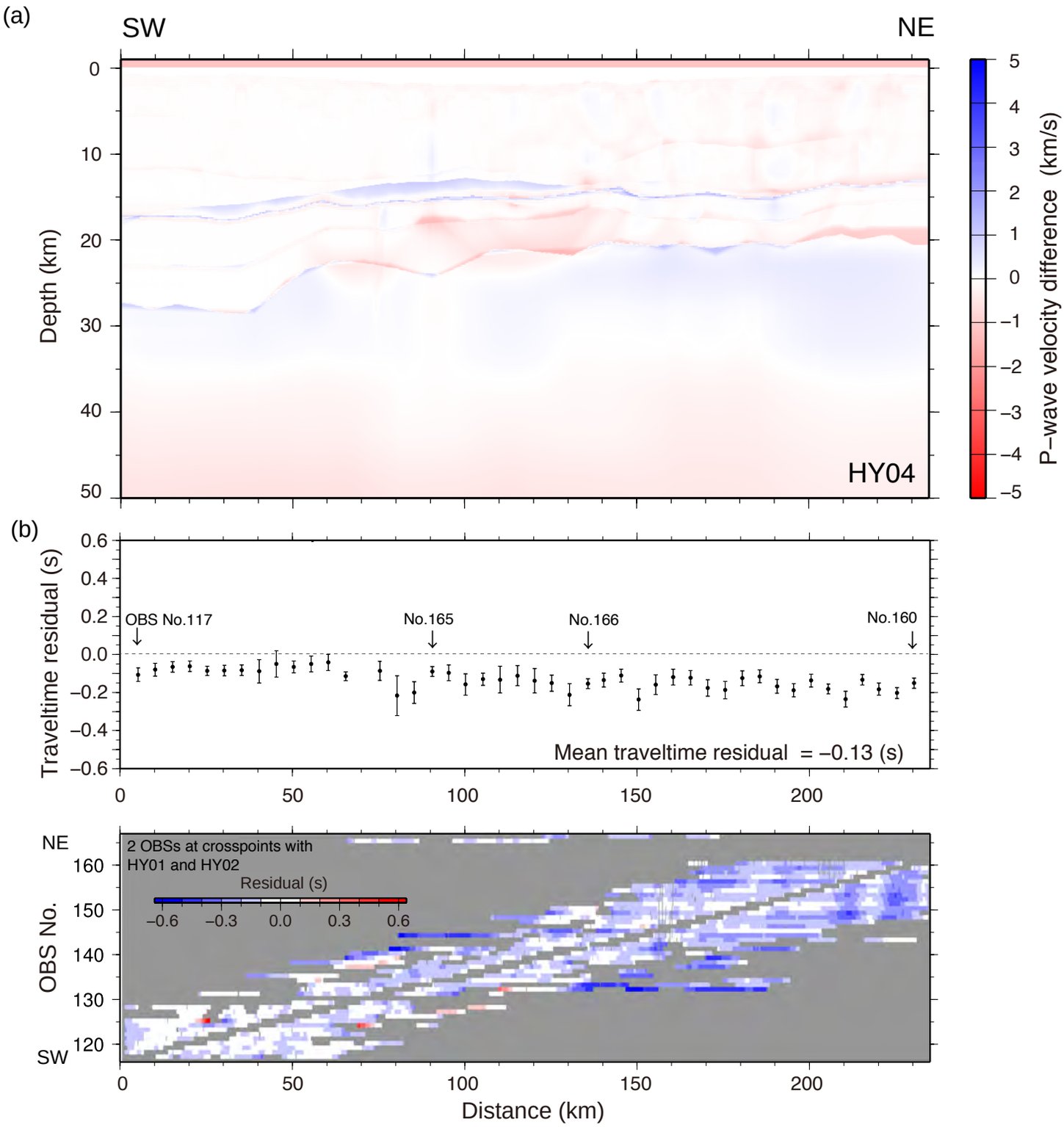
(a)
SW
NE
Depth (km)
HY04
P–wave velocity difference (km/s)
(b)
Traveltime residual (s)
OBS No.117
No.165
No.166
No.160
Mean traveltime residual = –0.13 (s)
NE
SW
OBS No.
2 OBSs at crosspoints with
HY01 and HY02
Residual (s)
Distance (km)

Figure S17

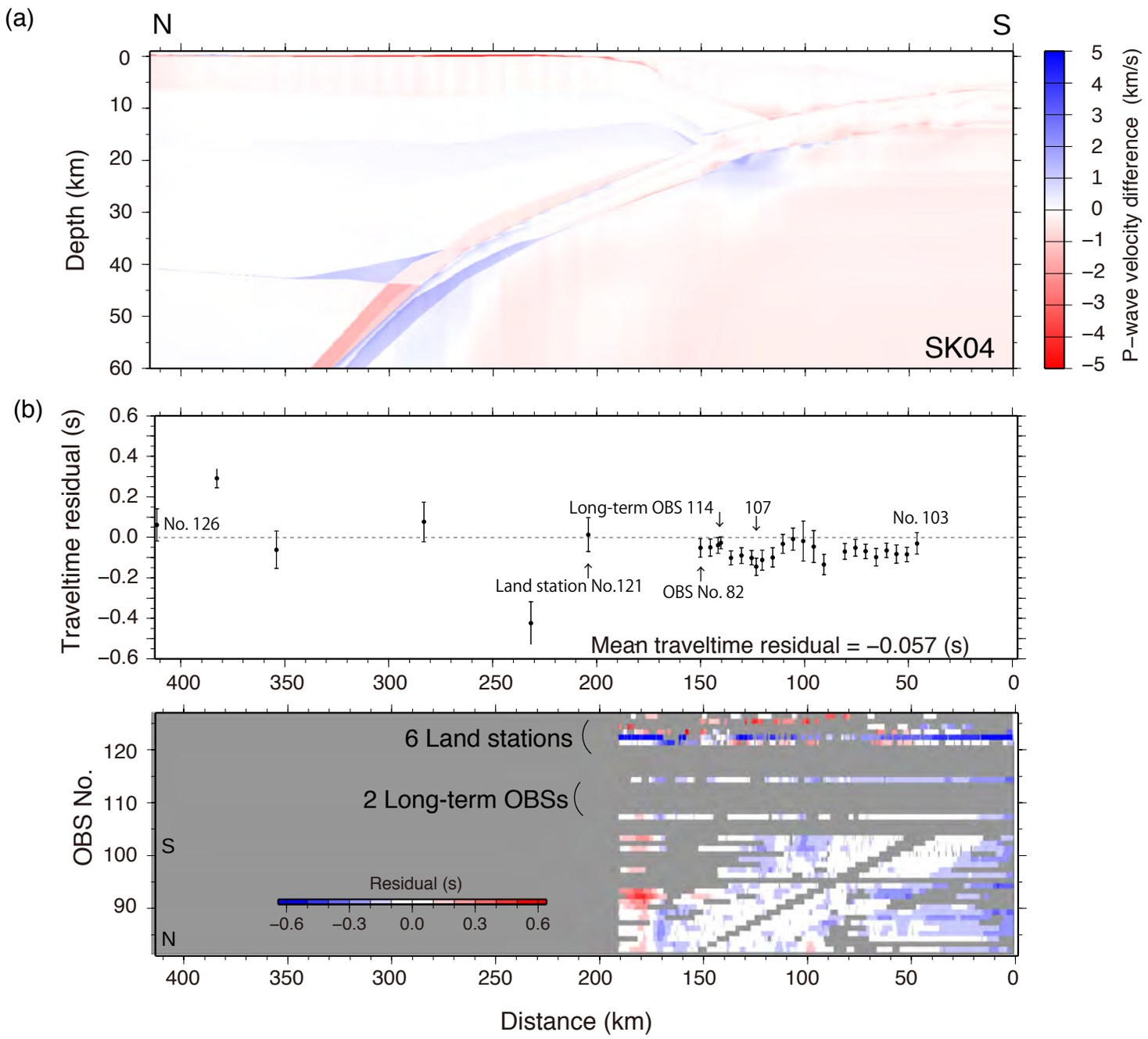
(a)
N
S
Depth (km)
SK04
P–wave velocity difference (km/s)
(b)
Traveltime residual (s)
No. 126
Long-term OBS 114
107
No. 103
Land station No.121
OBS No. 82
Mean traveltime residual = –0.057 (s)
6 Land stations
2 Long-term OBSs
OBS No.
S
N
Residual (s)
Distance (km)

Figure S18

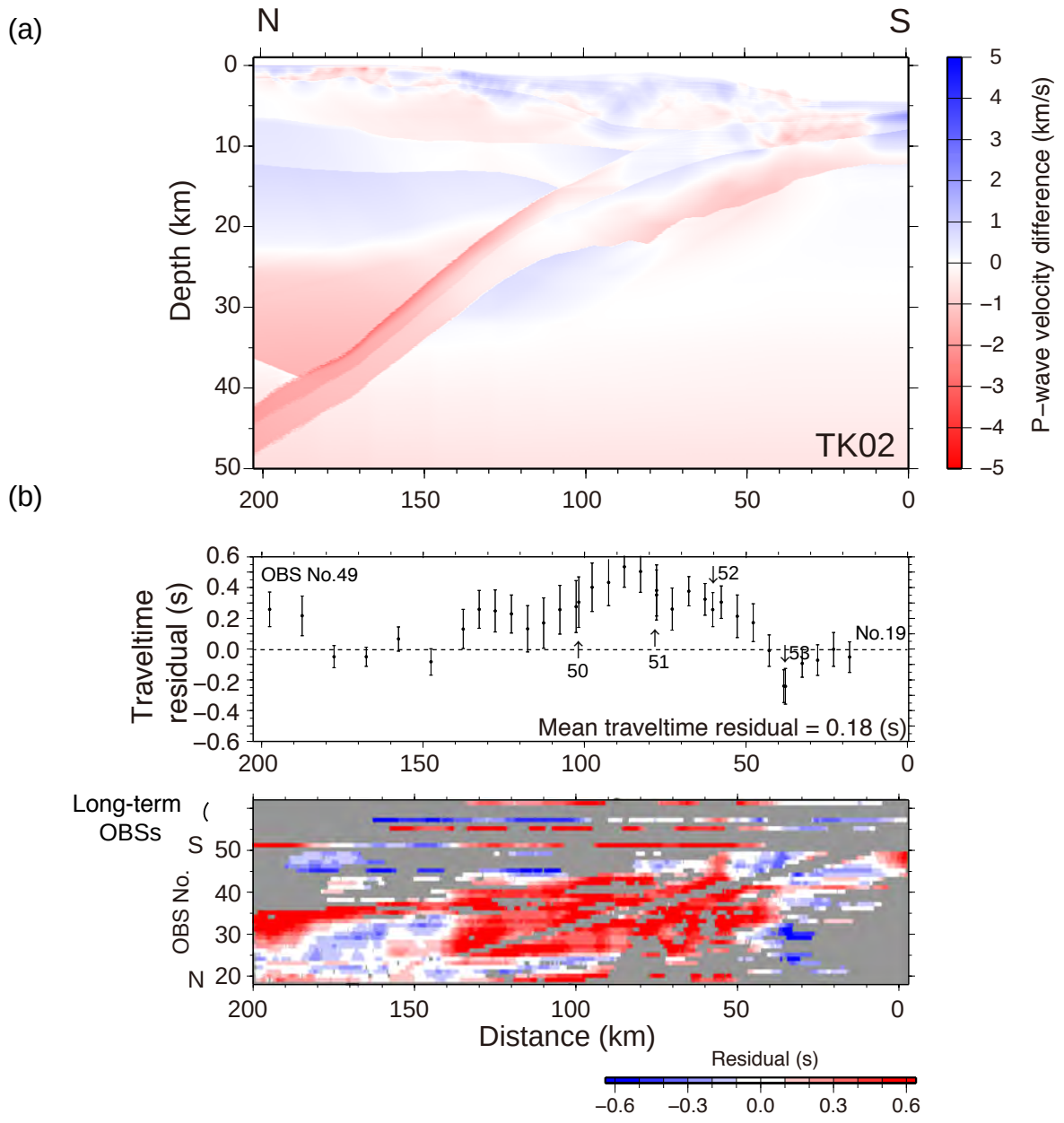
(a)
N
S
Depth (km)
TK02
P–wave velocity difference (km/s)
(b)
Traveltime residual (s)
OBS No.49
No.19
Mean traveltime residual = 0.18 (s)
Long-term OBSs
OBS No.
Distance (km)
Residual (s)

Figure S19

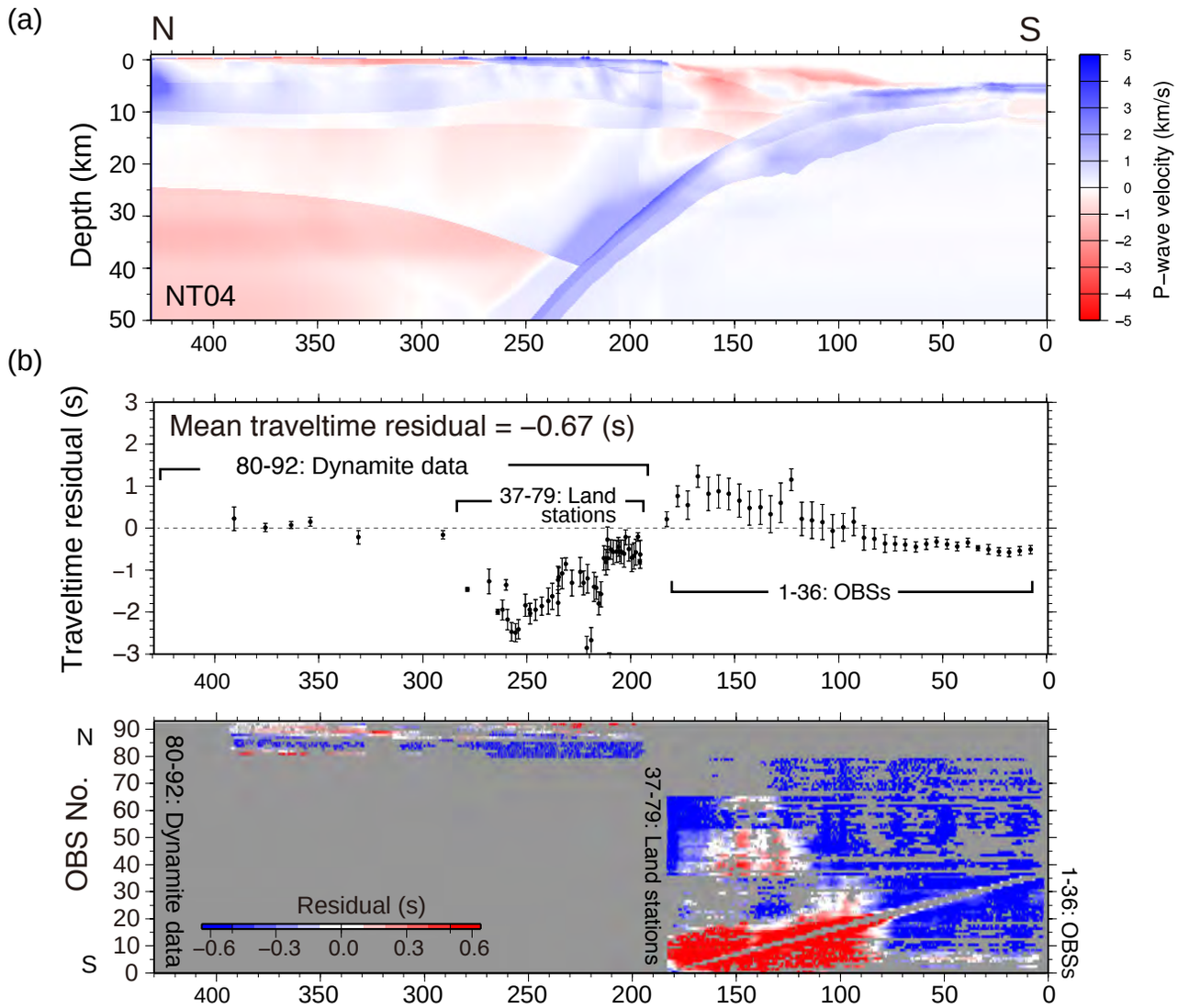
(a)
N
S
Depth (km)
NT04
P–wave velocity (km/s)
(b)
Traveltime residual (s)
Mean traveltime residual = –0.67 (s)
80-92: Dynamite data
37-79: Land stations
1-36: OBSs
OBS No.
N
S
80-92: Dynamite data
37-79: Land stations
1-36: OBSs
Residual (s)

Figure S20

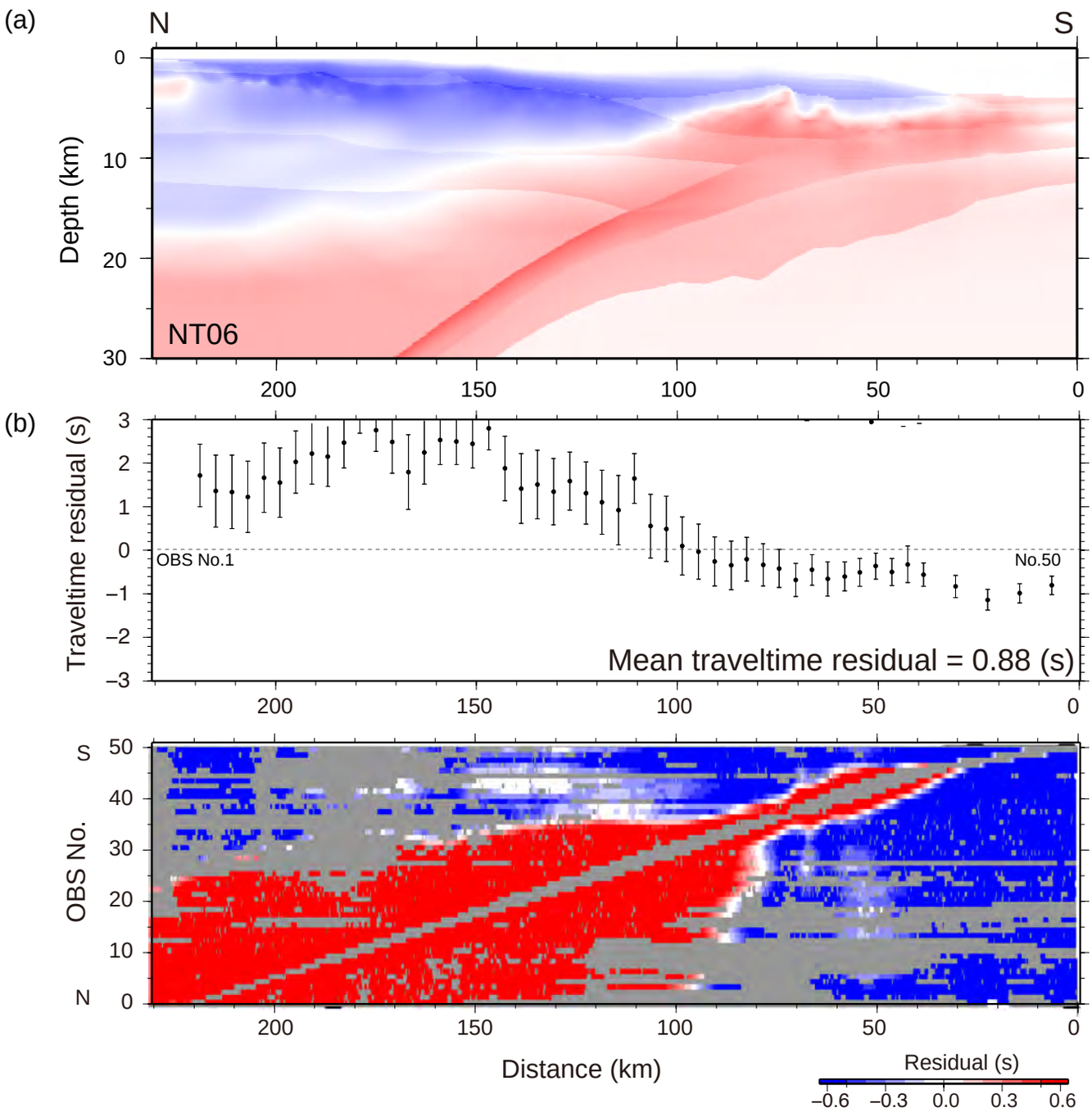
(a)
N
S
Depth (km)
0
10
20
30
NT06
200
150
100
50
0
(b)
Traveltime residual (s)
3
2
1
0
−1
−2
−3
OBS No.1
No.50
Mean traveltime residual = 0.88 (s)
200
150
100
50
0
OBS No.
S
N
50
40
30
20
10
0
200
150
100
50
0
Distance (km)
Residual (s)
−0.6
−0.3
0.0
0.3
0.6

Figure S21